

**CO(1-0), CO(2-1) and Neutral Gas in NGC 6946:
Molecular Gas in a Late-Type, Gas Rich, Spiral Galaxy**

Lucian P. Crosthwaite¹

Northrop Grumman, Unmanned Systems, San Diego, CA 92150

and

Jean L. Turner²

Division of Astronomy and Astrophysics, UCLA, Los Angeles, CA 90095

ABSTRACT

We present “On The Fly” maps of the CO(1-0) and CO(2-1) emission covering a $10' \times 10'$ region of the NGC 6946. Using our CO maps and archival VLA HI observations we create a total gas surface density map, Σ_{gas} , for NGC 6946. The predominantly molecular inner gas disk transitions smoothly into an atomic outer gas disk, with equivalent atomic and molecular gas surface densities at $R = 3.5'$ (6 kpc). We estimate that the total H_2 mass is $3 \times 10^9 M_{\odot}$, roughly 1/3 of the interstellar hydrogen gas mass, and about 2% of the dynamical mass of the galaxy at our assumed distance of 6 Mpc. The value of the CO(2-1)/CO(1-0) line ratio ranges from 0.35 to 2; 50% of the map is covered by very high ratio, > 1 , gas. The very high ratios are predominantly from interarm regions and appear to indicate the presence of wide-spread optically thin gas. Star formation tracers are better correlated with the total neutral gas disk than with the molecular gas by itself implying $\Sigma_{SFR} \propto \Sigma_{gas}$. Using the 100 μm and 21 cm continuum from NGC 6946 as star formation tracers, we arrive at a gas consumption timescale of 2.8 Gyr, which is relatively uniform across the disk. The high star formation rate at the nucleus appears to be due to a large accumulation of molecular gas rather than a large increase in the star formation efficiency. The mid-plane gas pressure in the outer ($R > 10$ kpc) HI arms of NGC 6946 is close to the value at the radial limit (10 kpc) of our observed CO disk. If the mid-plane gas pressure is a factor for the formation of molecular clouds, these outer HI gas arms should contain molecular gas which we do not see because they are beyond our detection limit.

Subject headings: ISM:molecules — stars:formation — galaxies:spiral — galaxies:ISM — galaxies:individual(NGC 6946)

¹ lpcrosthwaite@cox.net

² turner@astro.ucla.edu

1. Introduction

We have observed NGC 6946 as part of a program of deep mapping of extended, cold CO in nearby spiral galaxies (Crosthwaite et al. 2001, 2002). Large, fully-sampled, and deep images of CO in nearby galaxies are relatively uncommon. Interferometric images either do not contain zero spacing data (e.g., Sakamoto et al. 1999) or if they do, the images typically do not go deep enough to detect cold, molecular disk gas. The detection of cold, extended molecular gas at large galactocentric radii in large spirals is a goal of this mapping project with the NRAO 12 Meter Telescope.

A gas-rich Sc galaxy at a distance of 6 Mpc (Eastman et al. 1996; Sharina et al. 1997; Karachentsev et al. 2000), NGC 6946 is known for its bright and asymmetric optical spiral arms (Arp 1966). The pronounced asymmetry may be caused by interactions with neighboring dwarf galaxies, UGC 11583 and L149 (Sharina et al. 1997; Pisano & Wilcots 2000). NGC 6946 has a $9'$ optical diameter on the sky and an atomic hydrogen (HI) gas disk extending to $25'$ (Rogstad et al. 1973). Like many spirals, NGC 6946 has a central $\sim 2'$ diameter “hole” in its HI disk. Radio continuum, far infrared (FIR), optical line, and X-ray observations indicate vigorous star formation in the disk and an interstellar medium (ISM) stirred by supernovae and stellar winds (Engargiola 1991; Boulanger & Viallefond 1992; Kamphuis & Sancisi 1993; Schlegel 1994; Lacey et al. 1997). The high level of star formation in the disk of NGC 6946 has been attributed both to its strong spiral density wave (Tacconi & Young 1990), and to stochastic, self-propagating, star formation (DeGioia-Eastwood et al. 1984).

Until recently, the CO morphology beyond the inner $3'$ radius (~ 5 kpc) was not well known. Like many spiral galaxies, NGC 6946 has a bright nuclear CO peak which falls off nearly exponentially with galactocentric radius (Morris & Lo 1978; Young & Scoville 1982). A $3'$ diameter map of Tacconi & Young (1989) revealed substantial CO emission in the inner disk with several emission peaks. Casoli et al. (1990) mapped two $2'$ circular fields in the disk of NGC 6946 in a study of arm and interarm regions. The inner $2'$ region has been mapped with higher resolution single dish and aperture synthesis telescopes in transitions of CO and CO isotopomers (Ball et al. 1985; Weliachew et al. 1988; Sofue et al. 1988; Ishizuki et al. 1990; Wall et al. 1993; Regan & Vogel 1995). A larger interferometer+single dish map of NGC 6946 has been made by the BIMA SONG team (Regan et al. 2001), although with lower sensitivity to cold extended emission than the maps we present here. Walsh et al. (2002) presented $21''$ resolution fully-sampled single dish maps of CO(1-0). We compare our results to theirs.

The “On The Fly” (OTF) observing mode at the NRAO¹ was ideally suited to the imaging of extended gas in galaxies. Here, we present $16'$ by $10'$ maps of CO(1-0) and CO(2-1) covering the optical disk of NGC 6946 made with the 12 Meter Telescope. The maps are deep enough to detect cold, extended interarm CO to levels of $I_{CO} \sim 1$ K km s⁻¹, or $N_{H_2} \sim 2 \times 10^{20}$ cm⁻². We use these

¹The National Radio Astronomy Observatory is a facility of the National Science Foundation operated under cooperative agreement by Associated Universities, Inc.

primary tracers of the molecular gas phase and combine them with archival and published data in order to study the molecular gas disk, the total neutral gas surface density, and their relationship to star formation in the disk of NGC 6946.

2. The Observations and Data Reduction

2.1. 12 Meter CO Observations

The observations of CO(1-0) at 115 GHz and CO(2-1) at 230 GHz were made at the NRAO 12 Meter Telescope at Kitt Peak, on two separate observing runs in December 1996 and March 1997. An equivalent of ~ 14 hours on-source observing was accumulated for each CO line. Calibration was by the chopper wheel method (Ulich & Haas 1976). We convert the recorded T_r^* values (Kutner & Ulich 1981) to main beam temperature, $T_{mb} = T_r^* / \eta_m^*$, $\eta_m^* = 0.88 \pm 0.04$ at 115 GHz and $\eta_m^* = 0.56 \pm 0.06$ at 230 GHz (Mangum 1996a, 1997)². We report $T_{co} = T_{mb}$ throughout this paper. The filter bank spectrometer was configured for 2 MHz channel widths with 256 total channels, producing spectral channels of a 5.2 km s^{-1} width at 115 GHz and 2.6 km s^{-1} at 230 GHz.

The ‘‘On The Fly’’ (OTF) observing mode was used (Mangum 1996b)³. Scanning rates between 30 and 40 ''/sec and scan row spacings of 18'' at 115 GHz and 8'' at 230 GHz were selected to ensure sampling better than Nyquist over the mapped $16' \times 10'$ region. The beamsize (FWHM) at 115 GHz is 55'' and 27'' at 230 GHz. Chopper wheel calibration and sky offs were measured every 2 scans. The rms noise level was reduced by averaging the 16 individual OTF maps made at 115 GHz and 10 individual OTF maps at 230 GHz.

The OTF data was gridded using the NRAO AIPS package. A linear baseline was removed from each spectrum. At this stage of the data reduction the background in the channel maps is uneven from one scan row to the next. This spatial variation, due to sky brightness fluctuations between successive off-source sky measurements, appears as ‘‘stripes’’ in the continuum level running in the scan direction. The maps were made large enough to give us emission free, 2.5' wide, regions at the east and west ends of the maps, verified by the examination of individual spectra from these regions. These regions were used to remove a linear baseline from each row of the channel maps in the scan direction, effectively giving us a uniform background in all the channel maps. The rms variation in the channel maps before and after ‘‘de-striping’’ differed by 10 mK at 115 GHz and 30 mK at 230 GHz; in both cases a 20% reduction in the channel map noise.

The mean rms noise (1σ) from fully reduced, line free channels is $T_{mb} = 0.050 \text{ K}$ and $T_{mb} = 0.145 \text{ K}$ for the CO(1-0) and CO(2-1) respectively. The channels were averaged to a 10.4 km s^{-1}

²Available at <http://www.tuc.nrao.edu/12meter/obsinfo.html>.

³Available at <http://www.tuc.nrao.edu/12meter/obsinfo.html>.

channel width; the mean rms noise in the averaged channel maps is 0.035 K for CO(1-0) and 0.085 K for CO(2-1). The error beam of the 12m Telescope, which has been measured at 345 GHz, is extrapolated to be 8-9' FWHM (Mangum 1997). The contributions from the error beam in the individual channel maps is estimated to be less than a few percent, which we neglect here (see discussion in Crosthwaite et al. 2002). In the 10.4 km s⁻¹ channel width cubes the rescaled uncertainty in T_{mb} due to sky brightness fluctuations is ± 7 mK for CO(1-0) and ± 11 mK for CO(2-1).

We are interested in bringing out as much of the extended low level CO emission as possible in our integrated intensity maps. To do this we want to minimize the noise that would normally be added to an I_{CO} map when the channel maps are added together. To test the effects of the level of flux cut (level in the individual channels below which the data is deemed to be noise and not added to the integrated map) on the final integrated flux, we did the following test. We convolved the CO cubes to twice the beam size and used the regions with emission $> 3 \sigma$ to create mask cubes. The mask cubes allow us to define areas of emission using smoothed, hence more sensitive images, which is one way of discriminating between signal and noise. We then created I_{CO} maps from both the masked and unmasked cubes using flux cuts from 1.0 σ to 0 σ in 0.1 σ decrements. The total flux in the CO(1-0) integrated intensity map made from the masked cube with a 0.5 σ flux cut agrees with flux from the unmasked cube with no flux cut, to within 1%. For the CO(2-1) map, a more conservative 0.8 σ was used.

We created maps of the per pixel uncertainty for our I_{CO} maps by combining the per channel sky brightness fluctuation and rms noise, counting the number of channels contributing to the integrated emission at each pixel, and then adding the uncertainty in η_m^* using error analysis techniques for the sums and products of independent variables. We created maps of the fractional uncertainty in our integrated intensity maps by dividing the aforementioned uncertainty maps by the I_{CO} maps themselves. The uncertainty is dominated at the nucleus by the uncertainty in η_m^* while at the outer edges of the maps the uncertainty is dominated by the rms noise. For the CO(1-0) integrated intensity map the combined uncertainty is on the order of 7% at the nucleus, 12% along the prominent spiral arm pattern, and 25% for the outer disk emission. For the CO(2-1) map the uncertainties are on the order of 11% at the nucleus, 20% along the spiral arm pattern, and 30% for the outer disk emission.

To obtain H₂ column densities from I_{CO} we applied the “standard conversion factor”, X_{CO} (Scoville & Sanders 1987; Young & Scoville 1991). X_{CO} is estimated to be accurate to a factor of two in the Milky Way disk (Solomon et al. 1987, and references therein), although it may overpredict N_{H_2} in the central arcminute of large spirals (Dahmen et al. 1998; Meier & Turner 2001). We assume that these uncertainties hold for NGC 6946 as well. We will adopt the standard conversion factor,

$$X_{CO} = N_{H_2}/I_{CO} = 2 \times 10^{20} \text{ cm}^{-2} (\text{K km s}^{-1})^{-1} ,$$

of Strong et al. (1988) throughout the remainder of the paper (a recent calibration by Hunter et al. 1997, finds a mean $X_{CO} = 1.6 \times 10^{20} \text{ cm}^{-2} (\text{K km s}^{-1})^{-1}$ for the entire Milky Way disk and

$X_{CO} = 2.7 \times 10^{20} \text{ cm}^{-2} (\text{K km s}^{-1})^{-1}$ for the outer disk, $R > R_{\odot}$). Using this conversion factor, I_{CO} can be converted into H_2 (no He or heavier elements) surface densities using

$$\Sigma_{\text{H}_2} (\text{M}_{\odot} \text{ pc}^{-2}) = 2.4 \times (I_{CO} / \text{K km s}^{-1})$$

including a geometric correction for inclination of the galaxy (40° , Table 1)⁴ to correct the surface densities to their face-on values.

2.2. HI, 21 cm Continuum and FIR Maps

We obtained archival VLA D array 21 cm observations of the HI line in NGC 6946, which are described in Tacconi & Young (1986). The beam size is $49'' \times 42''$, with $pa = 73^{\circ}$, and each channel has a velocity width of 10.3 km s^{-1} . The integrated intensity map was constructed from signals greater than $1.7 \text{ mJy beam}^{-1}$ (1.2σ). Absolute flux calibration error is on the order of the uncertainty in the flux of 3C 286, $< 5\%$. The single channel rms noise of $1.4 \text{ mJy beam}^{-1}$ corresponds to an HI column density of $7.7 \times 10^{18} \text{ cm}^{-2}$.

Integrated intensities were converted to face-on HI surface densities (no He or heavier elements) using,

$$\Sigma_{HI} = 3.3 \text{ M}_{\odot} \text{ pc}^{-2} (\text{Jy beam}^{-1} \text{ km s}^{-1})^{-1} \cdot I_{HI}.$$

From a comparison to the single dish observations of Gordon et al. (1968) we estimate 40% of the HI flux of NGC 6946 is missing from the VLA maps due to the lack of short baselines (emission extended over $15'$). If the missing flux exists as a screen across the disk of NGC 6946 it constitutes a missing uniform HI surface density of $\sim 1.2 \text{ M}_{\odot} \text{ pc}^{-2}$.

The total observed HI emission in the VLA maps amounts to $M_{HI} = 5 \times 10^9 \text{ M}_{\odot}$, not including missing under-sampled emission. Tacconi & Young (1986), using the same VLA HI data, obtained $3.9 \times 10^9 \text{ M}_{\odot}$, rescaled to $D = 6 \text{ Mpc}$. Their mass is probably slightly lower than ours because they used a higher flux cutoff to produce their integrated intensity map. Boulanger & Viallefond (1992) obtained $6.7 \times 10^9 \text{ M}_{\odot}$ (rescaled to 6 Mpc). Boulanger’s mass includes single dish observations merged with the Westerbork interferometer data to cover the short spacings and corrections for Milky Way absorption and emission. The difference between our mass and theirs, 33%, is in line with our estimate of the missing flux in the VLA map.

A Brandt rotation curve was fit to the HI radial velocities, for radii $< 10'$. Our resulting kinematic parameters, Table 1, are in good agreement with the rotation parameters found by Carignan et al. (1990). A total dynamical mass estimate based on the fit (see Table 1) is: $M_{dyn} = 1.9(\pm 0.6) \times 10^{11} \text{ M}_{\odot}$.

⁴The adopted inclination was derived from a Brandt model fit to the HI data.

We produced a 21 cm continuum map by averaging 4 “line free” channels in the NGC 6946 HI channel cube. The 1σ noise level is $1.2 \text{ mJy beam}^{-1}$.

High resolution (HiRes) 60 and 100 μm IRAS maps were obtained from IPAC⁵. The 100 μm HiRes map was produced by 200 iterations of a maximum entropy method yielding a $69'' \times 65''$, $pa = 20^\circ$ beam and a 1σ noise level of 2.0 MJy sr^{-1} . The 60 μm HiRes map was produced by 50 iterations of a maximum entropy method yielding a $45'' \times 41''$, $pa = 21^\circ$ beam and a 1σ noise level of 0.6 MJy sr^{-1} .

3. Images of CO in NGC 6946: The Molecular Gas

A relatively heavy molecule, CO is easily excited at the temperatures of molecular clouds, with its first rotational level at an energy of $E/k = 5.5 \text{ K}$. Since it has a small dipole moment and is generally optically thick, the excitation of the CO rotational levels is driven by collisions at H_2 densities above $n_{crit} \sim 300 \text{ cm}^{-3}$ for the $J=1-0$ transition. The $J = 2-1$ transition, with an upper level energy of $E/k = 16.6 \text{ K}$, has a higher critical density, although its higher optical depth somewhat compensates for that. For gas kinetic temperatures of $\sim 7-10 \text{ K}$, we expect CO(2-1) to be thermalized at critical densities above $n_{crit} \sim 10^3 \text{ cm}^{-3}$, slightly higher than CO(1-0) values. One might therefore expect CO(2-1) emission to be more tightly confined to the spiral arms than CO(1-0), since the arms probably have denser gas, and are also closer to HII regions that might warm the clouds (e.g., Scoville et al. 1987). However, as we shall see, the CO(2-1) and CO(1-0) properties in NGC 6946 are not precisely what one might expect based on Galactic clouds.

We do not present CO kinematic data (radial velocity maps, velocity dispersion maps, rotation curves). Our kinematic results do not differ significantly from those of Walsh et al. (2002), and we refer the reader to their presentation of the kinematics of NGC 6946 derived from IRAM single dish data.

3.1. CO(1-0) Maps

The 24 CO(1-0) channels containing line emission are displayed in Figure 1. The channels have been smoothed to a 10.4 km s^{-1} channel width. The channel maps show the butterfly pattern characteristic of emission from an inclined rotating disk. High velocity nuclear gas shows up as emission at the location of the nucleus spread across nearly the entire bandwidth of the line emission.

The disk of CO emission in NGC 6946 extends $8'$ (14 kpc) north-south by $10'$ (18 kpc) east-west as shown in the integrated intensity, $I_{10} = \int T_{10} dv$ (Figure 2a), and the peak main beam brightness

⁵Descriptions of the IRAS HiRes data reduction and HiRes data products are available at <http://www.ipac.caltech.edu/ipac/iras/toc.html>.

temperature, T_{10} , (Figure 2b) maps. Walsh et al. (2002) also found CO emission extended out to $10'$ in $22''$ resolution single dish IRAM observations. There are no significant differences between our and Walsh’s map that cannot be attributed to the difference in resolution. The CO(1-0) emission covers the entire optical disk of a Digital Sky Survey (DSS) image of NGC 6946 (Figure 2c).

The total CO(1-0) flux density measured over a velocity width of 250 km s^{-1} is $1.2(\pm 0.3) \times 10^4 \text{ Jy km s}^{-1}$, in agreement with the value published in the FCRAO survey of $1.2(\pm 0.4) \times 10^4 \text{ Jy km s}^{-1}$ (Young et al. 1995), but higher than the $0.79(\pm 0.01) \times 10^4 \text{ Jy km s}^{-1}$ detected in a $22''$ resolution single dish IRAM map (Walsh et al. 2002). Converting our total observed I_{10} into a total molecular mass, we obtain $M_{H_2} = 3.3 \times 10^9 M_{\odot}$ for NGC 6946; the mass will be higher if there is outer disk CO that we do not detect. This is consistent with the mass obtained by Tacconi & Young (1989), $3.0 \times 10^9 M_{\odot}$ (rescaled to 6 Mpc and our X_{CO}).

The CO integrated intensity (I_{10}) and temperature maps (T_{10}) both show the same features: a bright nucleus, a broad asymmetrical spiral arm pattern and the overall asymmetrical distribution of the disk emission. The nucleus has a CO emission peak at $\alpha = 20^h 34^m 52.6^s$ $\delta = 60^\circ 9' 16''$ (J2000), with $I_{10}^{nuc} = 72 \text{ K km s}^{-1}$, $N_{H_2}^{nuc} = 1.4 \times 10^{22} \text{ cm}^{-2}$, or in terms of surface density, $\Sigma_{H_2}^{nuc} = 170 M_{\odot} \text{ pc}^{-2}$ (face-on value), averaged over our 1.6 kpc diameter beam. The total molecular mass within the central beam is $4.7 \times 10^8 M_{\odot}$. Ishizuki et al. (1990) obtained $4.5 \times 10^8 M_{\odot}$ (adjusted to 6 Mpc and our conversion factor) in a $65''$ diameter region from interferometric observations that recovered 70% of the total flux. Large scale CO spiral structure is traced in a broad “S” pattern, outlined by the 7.5 K km s^{-1} contour in the I_{10} map and more clearly seen in the T_{10} map, outlined by the 0.23 K contours. Here, molecular gas surface density is $> 20 M_{\odot} \text{ pc}^{-2}$. There is also extended, weaker CO emission from the disk outside of the 7.5 K km s^{-1} contour in the I_{10} map. Large regions of molecular gas exist to the northwest and southeast of the nucleus, as well as patchy emission out to the edges of the maps. Not all of this gas is associated with the weaker optical arm pattern. The face-on gas surface density for this extended region has a mean I_{CO} of $I_{10} \sim 3 \text{ K km s}^{-1}$ corresponding to $N_{H_2} = 5 \times 10^{20} \text{ cm}^{-2}$ or $\Sigma_{H_2} \sim 10 M_{\odot} \text{ pc}^{-2}$. This extended portion of the gas disk contributes 1/4 of the total CO emission we observe. The total mass of this extended gas disk is $M_{H_2} \sim 10^9 M_{\odot}$.

3.2. CO(2-1) Maps

The 24 channels containing CO(2-1) emission are displayed in Figure 3. The rms of these 10.4 km s^{-1} channels is three times as high as for CO(1-0), so the maps are less sensitive to faint emission. The total CO(2-1) flux density measured over a velocity width of 250 km s^{-1} is $3.5(\pm 1.0) \times 10^4 \text{ Jy km s}^{-1}$. The butterfly patterns for the CO(2-1) and CO(1-0) are generally the same, with the differing resolutions, $27''$ and $55''$ respectively, accounting for most of the differences.

As with CO(1-0) the bright nucleus and asymmetric distribution of arm and disk emission are also apparent in the integrated intensity, I_{21} , and peak main beam brightness temperature, T_{21} ,

maps (Figures 4a and 4b). The CO(2-1) emission in NGC 6946 is almost as extensive as that of the CO(1-0): the north-south and east-west dimensions are only 1' shorter. The observed CO(2-1) emission covers the brighter portions of the DSS optical image of NGC 6946, Figure 4c.

The nuclear peak of the CO(2-1) integrated intensity map is at $\alpha = 20^h34^m53.1^s$ $\delta = 60^\circ9'15''$ (J2000) with $I_{21}^{nuc} = 125$ K km s⁻¹. Using a Galactic disk X_{CO} , this corresponds to a peak column density of $N_{H_2}^{nuc} = 2.2 \times 10^{22}$ cm⁻² or 450 M_⊙ pc⁻² averaged over the 790 pc beam. If other nearby galaxies are any indication, this may be an overestimate of the true molecular gas mass in the nucleus, by factors of $\sim 2 - 3$ (§3.1.) The largest T_{21} value, 0.85 K, occurs at the same location as the I_{21} peak and both peaks are consistent with the location of the I_{10} peak.

At the resolution presented of maps, inside a 2' (3.5 kpc) radius both the CO(2-1) and CO(1-0) emission trace a broad 2 arm pattern. At a 2.5' radius (4.4 kpc) the CO(2-1) still traces a broad 2 arm pattern while the CO(1-0) emission from a larger beam has clearly bifurcated into a 4 arm spiral (Figure 5a). At a 3.5' radius (6.1 kpc) 5 arms are discernible in azimuthal emission plots of both CO emission lines (Figure 5b).

Along the optical arm pattern the CO(2-1) emission is uneven, (Figure 4c) with typical variations of 15 and 5 K km s⁻¹ separated by 40'' or less. This same clumpy pattern of CO arm emission can be seen in the 22'' CO(1-0) and CO(3-2) maps presented by Walsh et al. (2002). The emission on each arm at the same galacto-centric radius is also uneven as can be seen in Figures 5a and b.

At 27'' resolution it becomes possible to distinguish between arm and interarm emission. The I_{21} contrast between the brighter, on arm, clumps and obvious off-arm regions is ~ 3 . Using the DSS optical image to mask the outer (R > 2.5') arm/interarm regions, we obtain a mean arm/interarm contrast of 2.4. This is higher than both the 1.2 and 1.8 values found from CO(1-0) and CO(3-2) IRAM observations of Walsh et al. (2002) who interpret the increase in contrast at the higher CO transitions versus CO(1-0) as evidence that the on-arm molecular gas is warmer.

The presence of widespread interarm gas becomes plainly apparent in a comparison to an optical image, Figure 4c. The fact that interarm CO(2-1) is present and at emission levels comparable to CO(1-0) suggests that the interarm gas is also not very cold and that it must be warmer than $\sim 4 - 7$ K. This widespread distribution of interarm gas is not seen in the Sakamoto et al. (1997) CO(2-1) survey of the Milky Way.

3.3. Excitation of CO in NGC 6946

A CO ratio map, $r_{12} = I_{21}/I_{10}$, is presented in Figure 6a. The CO(2-1) channel cube was convolved to the beam size of the CO(1-0) data and the $> 3\sigma$ emission from the beam matched cubes was used to produce the r_{12} map. The spiral pattern is only weakly reflected in the r_{12} map. Outside of the inner few arcminute radius the pattern breaks up into a patchwork of high and low r_{12} regions.

The ratio uncertainty for the regions of strong emission is dominated by the error in the conversion to main beam temperature, while the uncertainty for the weaker emission regions is dominated by the rms noise in the contributing channels of emission. Adding in quadrature the fractional uncertainties from the I_{CO} maps we obtain an error estimate on the order of 15% at the nucleus, 25% along the spiral arm pattern, and 40% for the outer disk ratios. We were concerned that the ratio might be biased towards higher values due to the uncertainty in the denominator. We performed a standard statistical analysis to correct a ratio for bias this bias. The bias corrected r_{12} map was not significantly different from the map presented in Figure 6a and well within our reported error. Despite the large uncertainty estimates, our ratios are consistent with those derived from other independent observations (Weliachew et al. 1988; Ishizuki et al. 1990; Casoli et al. 1990; Wall et al. 1993).

In principle, r_{12} , the ratio of CO(2-1) to CO(1-0) integrated intensities, gives information on the excitation of the CO emission and depending on circumstances, the kinetic temperature, T_k . The observed main beam temperature at frequency, ν , is related to a Planck function, B_ν , with excitation temperature, T_{ex} , by the areal beam filling factor, f_a , a conversion to the Rayleigh-Jeans temperature scale, and radiative transfer through a optical depth, τ_ν :

$$T_{mb} = f_a \frac{c^2}{2k\nu^2} (B_\nu(T_{ex}) - B_\nu(T_{cmb})) (1 - e^{-\tau_\nu}),$$

including a correction for the cosmic microwave background contribution to the beam, $B_\nu(T_{cmb})$, at temperature 2.73 K. Standard assumptions are that f_a is the same for both emission lines, that both lines are optically thick ($\tau_\nu \gg 1$) and that the emission can be characterized by a single T_{ex} (Dickman et al. 1986; Maloney & Black 1988; Sakamoto 1996). With these assumptions we can naively derive T_{ex} values for the emission: $r_{12} = 0.9$ corresponds to $T_{ex} = 20$ K, while $r_{12} = 0.5$ corresponds to $T_{ex} = 3.5$ K. Higher ratio values are found in the nuclear regions of starburst galaxies where elevated star formation heats the molecular gas; lower values are typical of cold or subthermally excited ($T_{ex} < T_k$) disk molecular clouds. Values of $r_{12} > 1$ indicate optically thin gas in this picture.

Within $1'$ of the nucleus, $r_{12} \sim 0.8$. This is consistent with other studies (Weliachew et al. 1988; Ishizuki et al. 1990; Wall et al. 1993) that indicate the presence of relatively dense molecular gas as temperatures of about $T_{ex} \sim 10 - 15$ K. This is comparable to the Milky Way mean r_{12} of 0.74 (Oka et al. 1996, 1998).

Along the optical arms the mean r_{12} is 0.83, ranging from 0.44 to 1.4. To within our uncertainties, this is the same as the 0.73 mean found for Milky Way molecular arms where a similar range of r_{12} values is found (Sakamoto et al. 1995, 1997). From a naive interpretation of the ratios, a mean T_{ex} of 12 K is implied for the arm CO in NGC 6946.

Casoli et al. (1990) concluded that the interarm r_{12} does not differ significantly from that of the arms based on observations of two circular regions in the arms, one on the east side of NGC 6946, the other on the west side. The two circular regions they observed have a mean r_{12} of 0.8 in our

ratio map, also not significantly different from that of the arm regions. However when larger regions of the CO disk are sampled, a very different picture emerges. There are regions (5% of the ratio map) where $r_{12} < 0.6$ indicating cold ($T_{ex} < 5$ K) or sub-thermally excited CO. There are also much larger regions where $r_{12} > 1$.

Very high ratio, $r_{12} > 1$, gas covers 50% of our ratio map; and these are predominantly interarm regions, Figure 6b. We have eliminated the possibility that these very high ratios are due to contributions from the telescope error beam at 230 GHz: the error beam at the 12 Meter Telescope is a measured quantity and modeling of the error beam contribution in the individual channel maps shows that it contributes at most a few percent of the emission in the I_{21} map.

The high r_{12} ratios appear to indicate the presence of widespread, warm, optically thin CO-emitting gas in the interarm regions. While optically thin CO emission is not typical of Galactic molecular clouds, our large beam and unusual perspective from outside the disk of NGC 6946 may allow us to trace a component that is difficult to detect in the Galaxy. We note that the photon-dominated regions (PDR) around cool stars can produce bright CO emission with high temperatures (Spaans et al. 1994) since their softer radiation fields allow the CO to be photoelectrically-warmed at low A_v . Also, as pointed out by Wiklind et al. (1990) it does not take much optically thin gas to swing the emissivity; the CO(2-1) emission that we see could easily come from a small amount of optically thin, but “CO-loud” gas that is not the dominant cloud population. Other less likely possibilities are discussed in Crosthwaite et al. (2002).

We have also seen a have a high overall $r_{12} \sim 1$ in M83 (Crosthwaite et al. 2002); confirming earlier reports of unusually high r_{12} in these two galaxies (Castets et al. 1990; Wiklind et al. 1990). Large scale r_{12} maps of the Milky Way (Sakamoto et al. 1995; Oka et al. 1996; Sakamoto et al. 1997; Oka et al. 1998) show high ratios in immediate proximity to pockets of star formation. The widespread regions of high r_{12} seen in M83 and NGC 6946 are not seen in surveys of CO in our Galaxy.

4. CO, HI and the Neutral Gas Surface Density

Although CO emission covers only 15% of the HI disk surface area, NGC 6946 is nevertheless a molecular gas-rich galaxy; 1/3 of the hydrogen gas disk is in molecular form. This is consistent with the 36% value from Walsh et al. (2002) once the flux missed in the interferometer HI maps is taken into account.

In Figure 7a, we present our CO(1-0) emission in contours superimposed on a grey scale image of the HI emission. This image shows that CO emission fills the inner 6' of the HI disk. The HI disk has a central depression, which rises to peaks in a clumpy ring of emission. The HI ring is coincident with the outer boundary of CO(1-0). While spiral structure is readily apparent in the outer HI disk (Tacconi & Young 1986), it is insignificant in the inner disk, $R < 5'$ (9 kpc), where the HI column densities decline and H_2 takes over. At 1' resolution there are no obvious systematic

displacements of the HI relative to the CO(1-0) spiral structure other than the strongest HI tends to be near the outermost ends of the CO(1-0) arms. In fact, if anything, HI and CO peaks tend to coincide, which is more apparent in the higher resolution CO(2-1) maps.

The CO(2-1) image in contours is shown in Figure 7b, again with a grey scale image of HI. Outside the inner 2' (3.5 kpc) region of the HI depression, the peaks of CO(2-1) emission tend to coincide with HI peaks along the ring. This could be evidence for photodissociated H₂ creating a higher HI column density at these locations. Tilanus & Allen (1989, 1993) and Wilson & Scoville (1991) suggest the same explanation for HI in the spiral arms of M51, M83 and M33.

From these images, we have constructed plots of the azimuthally-averaged gas surface densities, Σ_{H_2} , Σ_{HI} and Σ_{gas} , as a function of galactocentric radius in Figure 8 (corrected for inclination). This is similar to the plot of Young & Scoville (1982), which was based on a radial cross map, and those of Tacconi & Young (1986) and Walsh et al. (2002). H₂ dominates the neutral gas distribution in within the central 3' (5 kpc) of NGC 6946, rapidly fading into a predominantly HI disk beyond. A least squares fit of an exponential to I_{CO} over the entire range of radii has a scale length of $1.0' \pm 0.1$ (1.8 kpc). Tacconi & Young (1986) and Walsh et al. (2002) obtained scale lengths of 1.5' and 1.4' for the CO disk from FCRAO and IRAM single disk observations; Regan et al. (2001) obtained 1.3' from the BIMA interferometer survey data combined with NRAO 12m observations. All these latter scale lengths exclude the nuclear contribution to the fit and are sensitive to the range of radii over which they computed. We obtain 1.2' and 1.3' fitting to the range of radii used by Tacconi & Young (1986) and Walsh et al. (2002), 40'' - 280'' and 60'' - 260'' respectively. We conclude that the CO falls off with an exponential scale length of $1.2' \pm 0.2'$ on arcminute scales, excluding the inner 1' nuclear region and about 1' if the nucleus is included.

A total neutral gas surface density map, $\Sigma_{gas} = 1.36 (\Sigma_{HI} + \Sigma_{H_2})$ is presented in Figure 9a. This map has been corrected for inclination but not for missing Σ_{HI} due to under-sampling in the VLA image ($\sim 1 M_{\odot} \text{ pc}^{-2}$). A false color image is presented in Figure 9b, with HI in red and CO in green, so that the molecular contribution to the total gas disk can be distinguished. Values for Σ_{gas} range from 240 $M_{\odot} \text{ pc}^{-2}$ at the nucleus, to 20-45 $M_{\odot} \text{ pc}^{-2}$ along the spiral arms within the optical part of the galaxy, to 5-10 $M_{\odot} \text{ pc}^{-2}$ for the outer arms. At first glance, H₂ and HI blend into a single global gas structure extending from the nucleus to the outer gas disk. A closer look reveals some subtleties. In the southern part of NGC 6946, the neutral density gradient is smooth and gradual. In the north, the gradient is much steeper, with the gas density falling to a level of 20 $M_{\odot} \text{ pc}^{-2}$ in 90'' (2.6 kpc) to the north, into an interarm void, as compared to a 180'' fall to the same mass density in the south (this can also be seen in Figures 7). This steeper falloff on the northern side of the central gas peak may be related to the more well-defined spiral arm to the north, and perhaps also to the prominent northeastern optical arm (Arp 1966).

The global properties of three late galaxies for which we have a similar data set, along with the Milky Way for reference are listed in Table 2. IC 342, M83 and NGC 6946 all have gas disks that extend well beyond their optical diameters and all three show some evidence for a bar. The $\Sigma_{H_2}^{disk}$

values for IC 342, NGC 6946 and M83 are all significantly higher than that of the Milky Way; a factor of four higher for IC 342 and NGC 6946, a factor of seven higher for M83. The NGC 6946 $\Sigma_{H_2}^{disk}$ value is similar to that of IC 342, while its $\Sigma_{H_2}^{nuc}$ intermediate between IC 342 and M83. All four galaxies have similar relative proportions of H₂ and HI, global M_{H_2}/M_{HI} values between 0.3 and 0.5 are also seen in the nearby galaxy, Maffei 2 (Mason & Wilson 2004). M83 stands out as a particularly gas-rich object relative to its dynamical mass, with a factor of two higher M_{gas}/M_{dym} than IC 342 and NGC 6946, and four times that of the Milky Way. The H₂ and optical disk diameters of the three external galaxies are the same, $D_{H_2}/D_{25} \sim 1$. The dynamical masses of these three galaxies are an order of magnitude smaller than that of the Milky Way, although their total gas mass is similar. It is difficult to place too much emphasis on subtle variations that rely on distance estimates, since the uncertain distances to these nearby galaxies can easily affect their masses, both gaseous ($\propto R^2$) and dynamical ($\propto R$).

5. Star Formation and the Neutral Gas Disk of NGC 6946

5.1. Star Formation Tracers, CO, and the Neutral Gas Disk

Because stars form from molecular gas, we expect to see correlations between CO and tracers of star formation. These tracers include: H α emission from ionized gas associated with massive young stars, FIR emission from dust heated by young stars, and radio continuum emission from relativistic electrons created by supernovae. To calculate linear correlation coefficients all the maps were convolved to the largest beam size in our collection of maps, a 70'' circular beam size, *then clipped to use $> 3\sigma$ emission*, and sampled on a 35'' grid.

H α emission (Ferguson et al. 1998) and I_{21} are compared in Figure 10a. The nuclear bar traced by H α within the central 2' is aligned with the elongation of the central I_{21} contours. The I_{21} arms are traced at higher resolution by the H α emission. In the outer I_{21} disk, the brighter patches of CO(2-1) emission are aligned with the brightest patches of H α which is most clearly seen along the northeastern spiral arms. This supports the conjecture that the ring of HI emission seen at these radii is the result of photodissociated H₂. It is apparent from this map that ratio of H α emission to I_{21} is not the same in the nucleus and outer arms; due to substantial extinction particularly in the nucleus, H α is probably not the optimal tracer of star formation for this gas-rich galaxy. When H α is compared to I_{21} or our primary molecular mass tracer, I_{10} , we obtain a linear correlation coefficient of ~ 0.65 . The H α correlations do not improve when a 1' diameter region centered on the nucleus is excluded from the correlation.

Figure 10b shows that the 60 μ m FIR emission generally reproduces the morphology seen in I_{21} (grey scale), despite the noticeable artifacts (the ‘‘boxy’’ structure of the central contours) produced by the HiRes maximum entropy algorithm. An ISOPHOT 60 μ m map by Tuffs et al. (1996) confirms the overall morphological structure seen in the HiRes map. The 60 μ m nuclear peak is at $\alpha = 20^h 34^m 52.4^s$ $\delta = 60^\circ 9' 15''$ (J2000) which is, within the uncertainties, coincident

with the CO peak. If CO(2-1) along with 60 μm FIR trace a warmer component both heated by star formation; we expect these emission pairs to have similar feature in the disk. The 60 μm emission traces the overall CO(2-1) arm structure better than the 100 μm emission shown in Figure 10c. The 4 prominent peaks in the outer 60 μm emission disk are aligned with peaks in the outer I_{21} arm structure.

The 100 μm FIR and 21 cm continuum maps have resolution comparable to our CO map (Figures 10c and d). The 100 μm emission roughly mimics the CO(1-0) emission disk, but the CO arm structure east of the nucleus is not well traced by the 100 μm . The 100 μm nuclear peak is at $\alpha = 20^{\text{h}}34^{\text{m}}53.0^{\text{s}}$ $\delta = 60^{\circ}9'23''$ (J2000); northeast of the CO emission peaks. The radio continuum does a better job reproducing the CO morphology, with the exception of the 21 cm peak 4' northwest of the nucleus. This is consistent with the suggestion that cosmic rays may be more important for the heating of molecular gas on large scales such as observed here than the radiation from in situ massive star formation (Adler, Allen, & Lo 1991; Suchkov et al. 1993). The continuum peak to the north and west of the nucleus at $\alpha = 20^{\text{h}}34^{\text{m}}24.9^{\text{s}}$ $\delta = 60^{\circ}10'38''$ is probably a background radio galaxy (van der Kruit et al. 1977, based on its spectral index, $\alpha = -0.84$ and flux.) The 21 cm continuum nuclear peak at $\alpha = 20^{\text{h}}34^{\text{m}}52.4^{\text{s}}$ $\delta = 60^{\circ}9'15''$ is consistent with the CO(1-0) peak. Much of the outer CO arm morphology and prominent emission peaks are traced by non-thermal radio continuum.

Walsh et al. (2002) also found statistically significant correlations between CO(1-0) emission and the total radio-continuum at 6 cm, and between CO(1-0) and 20 cm non-thermal continuum in NGC 6946. When fluxes are extrapolated to the expected 20 cm values (Condon 1992, using $S_{\nu} \propto \nu^{-0.8}$), we obtain a mean I_{10}/T_{20} of $1.4 \pm 0.5 \text{ km s}^{-1}$ from our 70'' beam convolved maps for the disk of NGC 6946. This is higher than the $I_{10}/T_{20} = 1.0$ value determined by Adler, Allen, & Lo (1991) from sparsely sampled I_{10} data, but in line with the 1.3 mean value for all the galaxies in their sample.

One might naively think that the FIR has a more direct causal link to newly formed stars, while radio continuum emission, which arises from relativistic electrons produced in supernova remnants, would be more spatially removed. In reality the far-infrared cirrus and non-thermal disk emission on arcminute scales represent a less temporally localized reflection of star formation; the close correspondence of radio continuum and CO supports a model of cosmic ray confinement on 1 kpc scale lengths. and highlights the importance of gas surface density in containing the magnetic field required to extract synchrotron emission from relativistic electrons (Bicay et al. 1989; Bicay & Helou 1990; Helou & Bicay 1993).

Table 3 lists least squares fits to the radial distribution of ratios of I_{10} or I_{21} to our star formation tracers, $G_{\text{tracer}}/SF_{\text{tracer}}$. With the exception of $\text{H}\alpha$, all the star formation tracers are highly correlated with CO emission. From the 70'' beam maps we obtain linear correlation coefficients on the order of ~ 0.95 or better in comparisons between either of our CO maps and any of the star formation tracers except for $\text{H}\alpha$. The radial gradient is reduced by a factor of two

when I_{10} is used instead of I_{21} indicating I_{10} remains the best tracer of molecular gas associated with star formation on kpc size scales.

While CO is highly correlated with star formation tracers, the correlation of total gas, HI+CO, is even better (see Table 3). The radial gradient is reduced by a factor of ten when Σ_{gas} is used. If we assume that the 21 cm and FIR emission trace star formation, this result implies that the star formation rate in NGC 6946 is more closely tied to Σ_{gas} than Σ_{H_2} . Restating this result: a simple Schmidt law applies, $SFE \propto \Sigma_{gas}^n$ (Schmidt 1959; Kennicutt 1998b), at least on kpc size-scales. *Moreover, it appears that in the outer parts of NGC 6946, star formation is likely to take place in regions of predominantly HI gas.*

We obtained similar results for IC 342 and M83 (Crosthwaite et al. 2001, 2002). While the correlation coefficient for Σ_{gas}/S_{21cm} in M83 is also high, 0.95, for IC 342 the correlation coefficient is only 0.73. The lower map correlation for IC 342 is related to the peculiar 1 armed appearance of the 21 cm continuum map that contrasts starkly with its grand design appearance in other tracers. From least squares fits to the Σ_{gas}/S_{21cm} ratio we obtain slopes of -0.012 ± 0.004 (dex) for IC 342 and -0.13 ± 0.02 (dex) for M83. For M83, the slope is not as flat as in IC 342 and NGC 6946. This gradient in M83 may indicate an age difference with larger Σ_{gas}/S_{21cm} values resulting from younger star forming regions in its disk (Suchkov et al. 1993). The Σ_{gas}/S_{21cm} comparison for NGC 6946 suffers none of these peculiarities.

A complication in the interpretation of molecular gas mass could arise because of a radial gradient in metallicity and because the Galactic CO conversion factor over-predicts the H_2 mass in the nucleus of NGC 6946 (Meier & Turner 2004). Based on the metallicity gradient for NGC 6946 measured by Belly & Roy (1992) and the metallicity adjustment to the CO conversion factor used by Wilson (1991) for giant molecular clouds in M33, X_{CO} could be a factor of two higher at the edge of the NGC 6946 CO disk. This would increase the molecular surface density derived from CO at the disk edge by a factor of two, and potentially reduce the radial gradient of molecular mass implied by I_{10} with radius. However, this variation in X_{CO} does not appear to be universal in low metallicity systems (Meier, Turner, & Beck 2002; Leroy et al. 2005), so we do not adopt the correction here.

5.2. The Star Formation Efficiency of the Disk of NGC 6946

Studies of the links between star formation and gas, or star formation efficiency, have recently focused on correlations as a function of position in the galaxy, as opposed to global measures. Rownd & Young (1999) examined the relation between Σ_{H_2} and the star formation rate, SFR, as traced by $H\alpha$; Murgia et al. (2002) compare a radio continuum based SFR and Σ_{H_2} ; Wong & Blitz (2002) compare a SFR from $H\alpha$ emission to Σ_{gas} . Young & Scoville (1982) pointed out that the falloff of Σ_{H_2} in NGC 6946 with radius was very similar to the falloff in B luminosity, implying a constant star formation rate per unit H_2 . The most widely used formulation is the Schmidt law,

$\Sigma_{SFR} = A \Sigma_{gas}^N$ (Schmidt 1959); and the most widely accepted calibration was done by Kennicutt (1998a) who finds $A = 2.5 \pm 0.7 \times 10^{-4}$ and $N = 1.4 \pm 0.15$ for Σ_{gas} in $M_{\odot} \text{ pc}^{-2}$ and Σ_{SFR} in $M_{\odot} \text{ yr}^{-1} \text{ kpc}^{-2}$. How well does the Schmidt law describe star formation in NGC 6946?

We can estimate star formation rates from our FIR and 21 cm continuum data. Unlike $H\alpha$ emission, these tracers are relatively unaffected by absorption. Although cirrus heated by an older population of stars may contaminate FIR in some galaxies, this is probably not a big effect in Scd type spirals (Sauvage & Thuan 1992). The 21 cm continuum appears to be a good star formation tracer on global scales, although it must break down at smaller scales. The maps for this analysis were convolved to the the largest circular beam in the set, $70''$.

We built a FIR map from the $60 \mu\text{m}$ and $100 \mu\text{m}$ IRAS maps using:

$$S_{fir} (\text{W m}^{-2} \text{ sr}^{-1}) = 12.6 \times 10^{-14} (2.58 S_{60\mu\text{m}} (\text{Jy sr}^{-1}) + S_{100\mu\text{m}} (\text{Jy sr}^{-1}))$$

(Catalogued Galaxies and Quasars in the IRAS Survey 1985). We adopt the FIR star formation rate:

$$\text{SFR}_{fir} (M_{\odot} \text{ yr}^{-1}) = 4.5 \times 10^{-37} L_{fir} (\text{W})$$

(Kennicutt 1998b), where $L = 4\pi D^2 S$ and D is the distance to NGC 6946. We derive the $\Sigma_{SFR_{fir}}$ map from the S_{fir} map using:

$$\Sigma_{SFR_{fir}} (M_{\odot} \text{ yr}^{-1} \text{ pc}^{-2}) = 5.38 \times 10^{-3} S_{fir} (\text{W m}^{-2} \text{ sr}^{-1}) \cos i$$

where $\cos(i = 40^\circ)$ gives us face-on surface values. For the non-thermal continuum at 21 cm we use

$$\text{SFR}_{ntc} (M_{\odot} \text{ yr}^{-1}) = 1.9 \times 10^{-22} \nu^{0.8} (\text{GHz}) L_{ntc} (\text{W Hz}^{-1})$$

to get the star formation rate (Condon 1992) and use:

$$\Sigma_{SFR_{ntc}} (M_{\odot} \text{ yr}^{-1} \text{ pc}^{-2}) = 2.30 \times 10^{-7} S_{1.42 \text{ GHz}} (\text{Jy beam}^{-1}) \cos i$$

to build the $\Sigma_{SFR_{ntc}}$ map. The Σ_{SFR} maps were azimuthally averaged in $30''$ radius bins.

The results are shown in Figure 11a. The SFRs derived from the FIR and radio continuum differ by a factor of two. Bell (2003) finds that the non-thermal continuum from low luminosity galaxies is substantially suppressed, and so calibrations of the SFR from radio continuum from surveys that do not take into account the overall luminosities of the constituent galaxies tend to underestimate the SFR. Bell provides an alternate calibration:

$$\text{SFR}_{ntc} (M_{\odot} \text{ yr}^{-1}) = \frac{5.5 \times 10^{-22}}{0.1 + 0.9(L/L_c)^{0.3}} L_{ntc} (\text{W Hz}^{-1})$$

where the total galactic flux satisfies the condition, $L \leq L_c$, $L_c = 6.4 \times 10^{21} \text{ W Hz}^{-1}$. In the case of NGC 6946, $L = 5.2 \times 10^{21} \text{ W Hz}^{-1}$. This calibration of SFR_{ntc} is also shown in Figure 11a and agrees with the FIR derived rate. Although the agreement with the SFR_{fir} result is clearly

promising, this alternate calibration was established using total galaxy fluxes and has not been studied with respect to the varying non-thermal continuum fluxes within galaxies. Figure 11a also shows the SFR predicted by the Kennicutt (1998a) calibration of the Schmidt law using our Σ_{gas} map; in NGC 6946, it overestimates the SFR relative the SFR_{fir} and SFR_{ntc} values.

Another way to look at the Schmidt law is in terms of the star formation efficiency, SFE. In Figure 11b we express the SFE for each of our SFRs as τ_{SFE} , the time it would take to consume all the gas at the given star formation rate, $\tau_{SFE} = \Sigma_{SFR}/\Sigma_{gas}$. Using the SFR_{fir} and Bell’s calibration for SFR_{ntc} , the mean τ_{SFE} for NGC 6946 is 2.8 ± 0.8 Gyr and $\Sigma_{SFR} \propto \Sigma_{gas}$. This is consistent with the mean τ_{SFE} of 2.6 Gyr for undisturbed galaxies found by Rownd & Young (1999). The $N = 1.4$ Schmidt law is also shown on Figure 11b; the Schmidt law over-predicts the SFE and its dependence on Σ_{gas} . Wong & Blitz (2002) found N values as low as 1.1 for the galaxies in their sample. Elmegreen (2002, see references within) has noted that the Schmidt law is inconsistent with observations that the SFE is roughly constant across range of galactic environments. This certainly is the case for NGC 6946.

On kpc scales, the SFE for the nucleus of NGC 6946 does not differ from that of the disk; in other words, the strong central FIR emission from the nucleus NGC 6946 results from having more molecular material from which to form stars rather than any increase in the star formation efficiency. This can be seen in Figure 12 where we show the radial distribution of the ratio of Σ_{gas} to 21 cm continuum; the ratio does not decline at the nucleus. The lowest values (highest efficiencies) are found between 2’ and 4’ radii (3.5 to 7 kpc). The highest values (lowest efficiencies) are at the largest radii. In two other late type galaxies for which we have a similar data set, IC 342 and M83, there is a noticeable drop in $\log(\Sigma_{gas}/S_{21cm})$ from the peak values in the disk to the nucleus; an indication of a elevated star formation efficiency relative to the disk rates (Crosthwaite et al. 2001, 2002). Using the definition of Rownd & Young (1999), NGC 6946 would not be a starburst galaxy because it does not have a gas cycling time shorter than 10^9 years. Other authors have come to a similar conclusion about the star formation efficiency in NGC 6946: Meier & Turner (2004) based on a determination of the nuclear molecular mass from high resolution observations of CO isotopes and multiple line transitions, and Madden et al. (1993) by evaluating the SFR using CII maps.

5.3. Is There an Edge to the CO Disk in NGC 6946?

Does the outer edge of our CO(1-0) map represent a real threshold for the formation of molecular clouds? Clearly in NGC 6946, there is not a steep or marked decline in the gas as we detected in M83; that galaxy has a real gas edge, in both CO and HI, possibly due to tidal interaction (Crosthwaite et al. 2002). In NGC 6946 the exponential disk continues as far as we can detect it (Figure 8). But there may be other subtle changes in the gas with radius and we examine these below.

We use our Galaxy as guide on what to expect for the radial falloff in gas and star formation

in a spiral galaxy. The number of HII regions per kpc^2 , Σ_{H_2} , and Σ_{HI} at R_\odot and 12 kpc (rescaled to $R_\odot = 8$ kpc) for the Milky Way from Wouterloot et al. (1988) are presented in Table 4. In the Galaxy, between 8 and 12 kpc N_{HII}/kpc^2 has fallen off by a factor of 15, Σ_{H_2} by a factor of 20, while Σ_{HI} stays relatively flat.⁶ Star formation per unit H_2 remains relatively constant over this range of radii. Wouterloot et al. (1988) found evidence for molecular outflows at distances as large as 16 kpc. Lequeux et al. (1993) detected Galactic molecular gas in a search for CO absorption lines against continuum sources; their findings suggest cold molecular gas may be far more abundant at large radii than previously suspected; they suggest the molecular gas mass may be 4 times the HI mass at 12 kpc. Mead & Kutner (1988) detect a sparse distribution of Milky Way molecular clouds at 13 kpc with a mean $T_r^* \sim 3$ K and a mean radius of 20 pc.

The edge of the observed CO disk in NGC 6946 lies midway between 8 and 12 kpc for an assumed distance of 6 Mpc. Comparing NGC 6946 to the Milky Way (Table 4): at 8 kpc ($4.6'$) N_{HII}/kpc^2 is a factor of four less in NGC 6946 than the Galactic value at R_\odot , and could be due to extinction in $H\alpha$. Σ_{H_2} is the same for both galaxies (within the errors), and Σ_{HI} is at least twice the Galactic value. At 12 kpc, N_{HII}/kpc^2 is the same as Galactic (extrapolating $20''$ in radius past the radial limit of the Hodge & Kennicutt (1983) data set), Σ_{H_2} is no longer detected in NGC 6946 by our observations, and Σ_{HI} is at least as large as the value for the Milky Way. We conclude that given the similarity of N_{HII}/kpc^2 and Σ_{HI} between these two galaxies, we would expect that Σ_{H_2} in NGC 6946 should be also be $> 0.1 M_\odot \text{pc}^{-2}$ at 12 kpc.

Complicating these comparisons is the uncertainty in the NGC 6946 distance. To date, there are no Cepheid-based distance estimates to NGC 6946, which has a low Galactic latitude. Recent estimates are (in Mpc): 5.7 ± 0.7 based on type II SN (Eastman et al. 1996), 6.4 ± 0.4 based on the brightest stars (Sharina et al. 1997), and 5.9 ± 0.4 based on blue supergiants (Karachentsev et al. 2000). As with any comparison based on absolute scales, our comparison changes if the the 6 Mpc distance estimate is incorrect by more than ± 0.5 Mpc.

The mapping of the CO disk presented here is sensitivity-limited; our 3σ detection limit is $2\text{-}3 M_\odot \text{pc}^{-2}$. A combination of low T_{ex} and a low filling factor for molecular clouds in the beam combine to create a detection limit rather than a real threshold. There is also the possibility that declining metallicity in the outer disk lowers the CO emissivity relative to N_{H_2} , although this effect has yet to be seen. There are probably clouds here, but more widely dispersed than they are in the inner parts of the NGC 6946.

But our suspicion that there is substantial molecular gas at large galactic radii is not based entirely on a comparison to the Milky Way. There are theoretical reasons to expect molecular gas at radii beyond our detected CO edge (Elmegreen 1989, 1993; Elmegreen & Parravano 1994; Honma et al. 1995). According to Elmegreen & Parravano (1994) molecular clouds are not formed

⁶Caveat: these are not azimuthal averages, but rather represent volumes at the sun and a variety of viewing angles centered on a Galactic anticenter vector, and may not be representative of the Galaxy as a whole.

where the ISM pressure, P_{ism} , becomes too low to facilitate the formation of cold, dense clouds. Or conversely, molecular clouds form in regions where $P_{ism} > P_{min}$. The outer HI disk of NGC 6946 has considerable surface density structure that exists on kpc in-plane size scales and where P_{ism} may locally exceed this minimum. To calculate the mid-plane gas pressure we use:

$$P_{ism} = 0.5 \pi G \Sigma_{gas}^2$$

where we have ignored the stellar contribution to the pressure which can only act to increase the value (Elmegreen & Parravano 1994). Along the outer ($R \sim 6'$, 10 kpc) HI gas arms, $P_{ism} \sim 2 \times 10^3 \text{ cm}^{-3} \text{ K}$ which is close to P_{ism} values at the edge of the CO disk. The outer gas arms are where one would expect to find molecular gas, if we had deeper maps. Several of the HII regions identified by Hodge & Kennicutt (1983) are located beyond the edge of our CO disk, particularly to the south, and it is likely that they are associated with molecular clouds that are too beam-diluted and cold to show up in our images. Ferguson et al. (1998) have detected $H\alpha$ emission associated with the formation of massive stars, up to $3'$ beyond our CO disk edge and precisely at the local maxima in the outer HI arms of NGC 6946. These star forming outer arms would be good places to look for CO with a smaller beam and higher sensitivity.

Based on theoretical arguments and the detection of $H\alpha$ in NGC 6946 at large galactic radii, the answer is: no, the “edge” of the CO disk at a galactocentric radius of $5'$ ($\sim 9\text{-}10$ kpc) in our images is not a real edge, it is a detection limit. There is no significant change in properties to indicate that the disk is undergoing a change at this radius. There could easily be molecular clouds that escape detection beyond this radius

6. Conclusions

We have obtained deep CO(1-0) and CO(2-1) images of a $10' \times 10'$ region centered on the Sc galaxy, NGC 6946, with $55''$ and $27''$ resolution using the NRAO 12 Meter Telescope. We have combined these deep CO images with VLA HI images to obtain images of the neutral gas in this galaxy. To summarize our findings:

- 1) The CO(1-0) and CO(2-1) disks shows many of the same features seen in the optical disk: a strong nuclear peak of emission, molecular gas arms spatially coincident with the asymmetric optical arm pattern, and a $10'$ diameter inner disk filled with CO emission. The CO disk is roughly exponential with a scale length of $1.2' \pm 0.2'$ or 2 ± 0.3 (D/6 Mpc) kpc.
- 2) We obtain 3.3×10^9 (D/6 Mpc) $^2 M_{\odot}$ for the molecular hydrogen gas mass of NGC 6946. This can be compared to the total atomic hydrogen gas mass of $M_{HI} = 7.0 \times 10^9$ (D/6 Mpc) $^2 M_{\odot}$ (which includes a VLA missing flux estimate). Molecular hydrogen constitutes 1/3 of the interstellar hydrogen gas mass and 2% of the dynamical mass of NGC 6946. At the nucleus, $\Sigma_{H_2} = 170 M_{\odot} \text{ pc}^{-2}$, the molecular gas surface density is $> 20 M_{\odot} \text{ pc}^{-2}$ along the strong optical arm pattern, and $\sim 10 M_{\odot} \text{ pc}^{-2}$ regions beyond.
- 3) The mean value for $r_{12} = I_{CO(2-1)}/I_{CO(1-0)}$ in the the nucleus and optical arm pattern is

$\sim 0.83 \pm 0.14$. This is consistent with optically thick gas, with an excitation temperature of 10-15 K. Interarm CO shows the largest variation in r_{12} , with a range of 0.35 to 2. Only 4% of the CO ratio map has $r_{12} < 0.6$ which is likely to be cold or subthermally excited CO ($T_{ex} < 4$ K). Fully half of the CO disk of NGC 6946 has $r_{12} > 1$. The high r_{12} appears to indicate the presence of widespread, optically-thin gas in between the spiral arms.

4) Molecular gas dominates the total gas surface density within a galactocentric radius of $3.5'$ (6 kpc). CO emission fills the central depression in the HI disk. Beyond the nuclear region, there is a good correlation between the CO and HI gas, which both peak on the spiral arms. The inner disk arm pattern transitions smoothly from predominantly CO arms to predominantly HI arms at the outskirts of the CO disk. At the nucleus, $\Sigma_{gas} = 240 M_{\odot} \text{ pc}^{-2}$, the total gas surface density is $> 20 - 45 M_{\odot} \text{ pc}^{-2}$ along the optical arm pattern, and $\sim 5 - 10 M_{\odot} \text{ pc}^{-2}$ along the outer gas arms ($\Sigma_{gas} = 1.36(\Sigma_{H_2} + \Sigma_{HI})$). CO(2-1) emission peaks are coincident with clumps of HI, H α , and FIR emission outside the nuclear region, presumably an indication of warmer molecular gas and dissociated H $_2$.

5) We find strong correlations between star formation tracers (except for H α) and CO emission in NGC 6946. The correlation coefficients are ~ 0.95 . When Σ_{gas} is used instead of just the molecular gas tracer in a radial comparison, the dependence on galactic radius is reduced. Star formation is more closely related to the total gas surface density than the molecular gas surface density alone, a Schmidt law relationship. This also implies star formation is likely well beyond the radial limits of our observed CO disk in regions of predominantly HI gas. Surprisingly, H α is not as well correlated with CO or Σ_{gas} as are the other star formation tracers. The correlation coefficient is significantly less, ~ 0.65 , and the ratio formed from H α and CO or Σ_{gas} declines more rapidly with galactic radius.

6) The star formation efficiency in the disk of NGC 6946 is relatively uniform; 2.8 Gyr when expressed in terms of the gas consumption time-scale. This uniformity implies $\Sigma_{SFR} \propto \Sigma_{gas}$. The star formation rate at the nucleus is due to the high molecular surface density rather than an elevated star formation efficiency.

7) The edge of the observed CO disk represents a detection limit rather than a threshold for molecular cloud formation. We suspect the exponential fall of the CO disk continues smoothly past our detection limit. The mid-plane gas pressure in the outer HI arm structure, $P_{ism} \sim 2 \times 10^3 \text{ cm}^{-3} \text{ K}$ is close to the value at the limits of the observed CO disk. These gas arms should support the formation of molecular clouds which could be detectable in higher resolution observations.

The authors would like to thank the NRAO 12m telescope operators, Duane Clark, Paul Hart, Victor Gasho and Harry Stahl, for their help and company during the many observing sessions in which the data for NGC 6946 and other galaxies were acquired. We thank L. Tacconi giving for us permission to retrieve and use the HI 21 cm line observations from the VLA archive. And we appreciate the careful reading and critical suggestions made by the anonymous referee. This work was supported in part by NSF grants AST00-71276 and AST03-07950. We made use of the NASA/IPAC/IRAS HiRes data reduction facilities as well as STScI Digital Sky Survey facilities.

The Digitized Sky Surveys were produced at the Space Telescope Science Institute under U.S. Government grant NAG W-2166.

REFERENCES

- Adler, D. S., Allen, R. J., & Lo, K. Y. 1991, ApJ, 283, 475
- Arp, H. 1966, ApJS, 14, 1
- Arsenault, R. 1989, A&A, 217, 66
- Ball, R., et al. 1985, ApJ, 298, L21
- Bell, E.F. 2003, ApJ, 586, 794
- Belley, J. & Roy, J. 1992, ApJS, 78, 61
- Bicay, M.D., Helou, G. & Condon, J.J. 1989, ApJ, 338, L53
- Bicay, M.D. & Helou, G. 1990, ApJ, 362, 59
- Boulanger, F. & Viallefond, F. 1992, A&A, 266, 37
- Carignan, C., et al. 1990, A&A, 234, 43
- Casoli, F., et al. 1990, A&A, 233, 357
- Castets, A., et al. 1990, A&A, 234, 469
- Catalogued Galaxies and Quasars in the IRAS Survey 1985, prepared by Lonsdale, C.J., et al. (JPL)
- Combes, F. 1991, ARA&A, 29, 195
- Condon, J.J. 1992, ARA&A, 30, 575
- Crosthwaite, L.P., et al. 2001, AJ, 122, 797
- Crosthwaite, L.P., et al. 2002, AJ, 123, 1892
- Dahmen, G., et al. 1998, A&A, 331, 959
- DeGioia-Eastwood, K., et al. 1984, ApJ, 278, 564
- de Vaucouleurs, G., de Vaucouleurs, A. & Corwin, H. 1976, *Second Reference Catalogue of Bright Galaxies*, Univ. of Texas Press
- Dickman, R.L., Snell, R.L. & Schloerb, F.P. 1986, ApJ, 309, 326
- Eastman, R.G., et al. 1996, ApJ, 466, 911
- Elmegreen, B.G. 1989, ApJ, 338, 178
- Elmegreen, B.G. 1993, ApJ, 411, 170
- Elmegreen, B.G. 2002, ApJ, 577, 206
- Elmegreen, B.G. & Parravano, A. 1994, ApJ, 435, L121
- Engargiola, G. 1991, ApJS, 76, 875
- Ferguson, A.M.N., et al. 1998, ApJ, 506, L19

- Gordon, K.J., Remage, N.H. & Roberts, M.S. 1968, *ApJ*, 154, 845
- Helou, G. & Bica, M.D. 1993, *ApJ*, 415, 93
- Hodge, P.W. & Kennicutt, R.C. 1983, *AJ*, 88, 296
- Honma, M., Sofue, Y. & Arimoto, N. 1995, *A&A*, 304, 1
- Hunter, S.D., et al. 1997, *ApJ*, 481, 205
- Ishizuki, S. et al. 1990, *ApJ*, 355, 436
- Kamphuis, J. & Sancisi, R. 1993, *A&A*, 273, L31
- Karachentsev, I.D., Sharina, M.E. & Hutchmeier, W.K. 2000, *A&A*, 362, 544
- Kennicutt, R.C. 1998a, *ApJ*, 498, 541
- Kennicutt, R.C. 1998b, *ARA&A*, 36, 189
- Kulkarni, S.R., & Heiles, C. 1987, in *Interstellar Processes*, ed. Hollenbach & Thronson, p. 87
- Kutner, M.L. & Ulich, B.L. 1981, *ApJ*, 250, 341
- Lacey, C., Duric, N. & Goss, W.M. 1997, *ApJS*, 109, 417
- Lequeux, J., Allen, R.J. & Guilleaume, S. 1993, *A&A*, 280, L23
- Leroy, A. et al. 2005, *ApJ*, 625, 763
- Madden, S.C. et al. 1993, *ApJ*, 407, 579
- Maloney, P. & Black, J.H. 1988, *ApJ*, 325, 389
- Mangum, J.G. 1996, *User's Manual for the NRAO 12m Millimeter-Wave Telescope*, NRAO 12m Publication
- Mangum, J.G. 1996, *On The Fly Observing at the 12m*, NRAO 12m Publication
- Mangum, J.G. 1997, *Equipment and Calibration Status for the NRAO 12m Telescope*, NRAO 12m Publication
- Mason, A. M., & Wilson, C. D. 2004, *ApJ*, 612, 860
- Mead, K.N. & Kutner, M.L. 1988, *ApJ*, 330, 399
- Meier, D.S. & Turner, J.L. 2004, *AJ*, 127, 2069
- Meier, D.S. & Turner, J.L. 2001, *ApJ*, 551, 687
- Meier, D.S., Turner, J.L., & Beck, S. C. 2002, *AJ*, 124, 877
- Morris, M. & Lo, K.Y. 1978, *ApJ*, 223, 803
- Murgia, M., et al. 2002, *A&A*, 385, 412
- Nikiforov, I.I., Petrovskaya, I.V. & Ninkovic, S. 2000, *Small Galaxy Groups, ASP Conference Series*, 209, 399
- Oka, T., et al. 1996, *ApJ*, 460, 334
- Oka, T., et al. 1998, *ApJ*, 493, 730
- Pisano, D.J. & Wilcots, E.M. 2000, *MNRAS*, 319, 821
- Regan, M.W. & Vogel, S.N. 1995, *ApJ*, 452, L21

- Regan, M.W. et al. 2001, ApJ, 561, 218
- Rogstad, D.H., Shostak, G.S. & Rots, A.H. 1973, A&A, 22, 111
- Rownd, B.K. & Young, J.S. 1999, AJ, 118, 670
- Saha, A, Claver, J. & Hoessel, J.G. 2002, AJ, 124, 839
- Sakamoto, S. 1996, ApJ, 462, 215
- Sakamoto, S., et al. 1995, ApJS, 100, 125
- Sakamoto, S., et al. 1997, ApJ, 486, 290
- Sakamoto, S., et al. 1999, ApJS, 124, 403
- Sauvage, M. & Thuan, T.X. 1992, ApJ, 396, L69
- Schlegel, E. M. 1994, ApJ, 434, 523
- Schmidt, M. 1959, ApJ, 129, 243
- Scoville, N. Z. & Sanders, D.B. 1987, in *Interstellar Processes*, ed. Hollenbach & Thronson, p 21
- Scoville, N. Z., et al. 1987, ApJS, 63, 821
- Sharina, M.E., Karachentsev, I.D. & Tikhonov, N.A. 1997, AstL, 23, 373
- Sofue, Y., et al. 1988, PASJ, 40, 511
- Solomon, P.M., et al. 1987, ApJ, 319, 730
- Spaans, M., et al. 1994, ApJ, 437, 270
- Strong, A.W. et al. 1988, A&A, 207, 1
- Suchkov, A., Allen, R.J. & Heckman, T.M. 1993, ApJ, 412, 542
- Tacconi, L.J. & Young, J.S. 1986, ApJ, 308, 600
- Tacconi, L.J. & Young, J.S. 1989, ApJS, 71, 455
- Tacconi, L.J. & Young, J.S. 1990, ApJ, 352, 595
- Tilanus, R.P.J. & Allen, R.J. 1989, ApJ, 339, L57
- Tilanus, R.P.J. & Allen, R.J. 1993, A&A, 274, 707
- Tuffs, R.J. et al. 1996, A&A, 315, L149
- Ulich, B.L. & Hass, R.W. 1976, ApJS, 30, 247
- van der Kruit, P.C., Allen, R.J. & Rots, A.H. 1977, A&A, 55, 421
- Wall, W.F., et al. 1993, ApJ, 414, 98
- Walsh, W., et al. 2002, A&A, 388, 7
- Weliachew, L., Casoli, F. & Combes, F. 1988, A&A, 199, 29
- Wiklind, T., et al. 1990, A&A, 232, L11
- Wilson, C.D. 1995, ApJ, 448, L97
- Wilson, C.D. & Scoville, N. 1991, ApJ, 370, 184
- Wong, T. & Blitz, L. 2002, ApJ, 569, 157
- Wouterloot, J.G.A., Brand, J. & Henkel, C. 1988, A&A, 191, 323

Young, J.S. & Scoville, N.Z. 1982, ApJ, 258, 467

Young, J.S. & Scoville, N.Z. 1991, ARA&A, 29, 581

Young, J.S., et al. 1995, ApJS, 98, 219

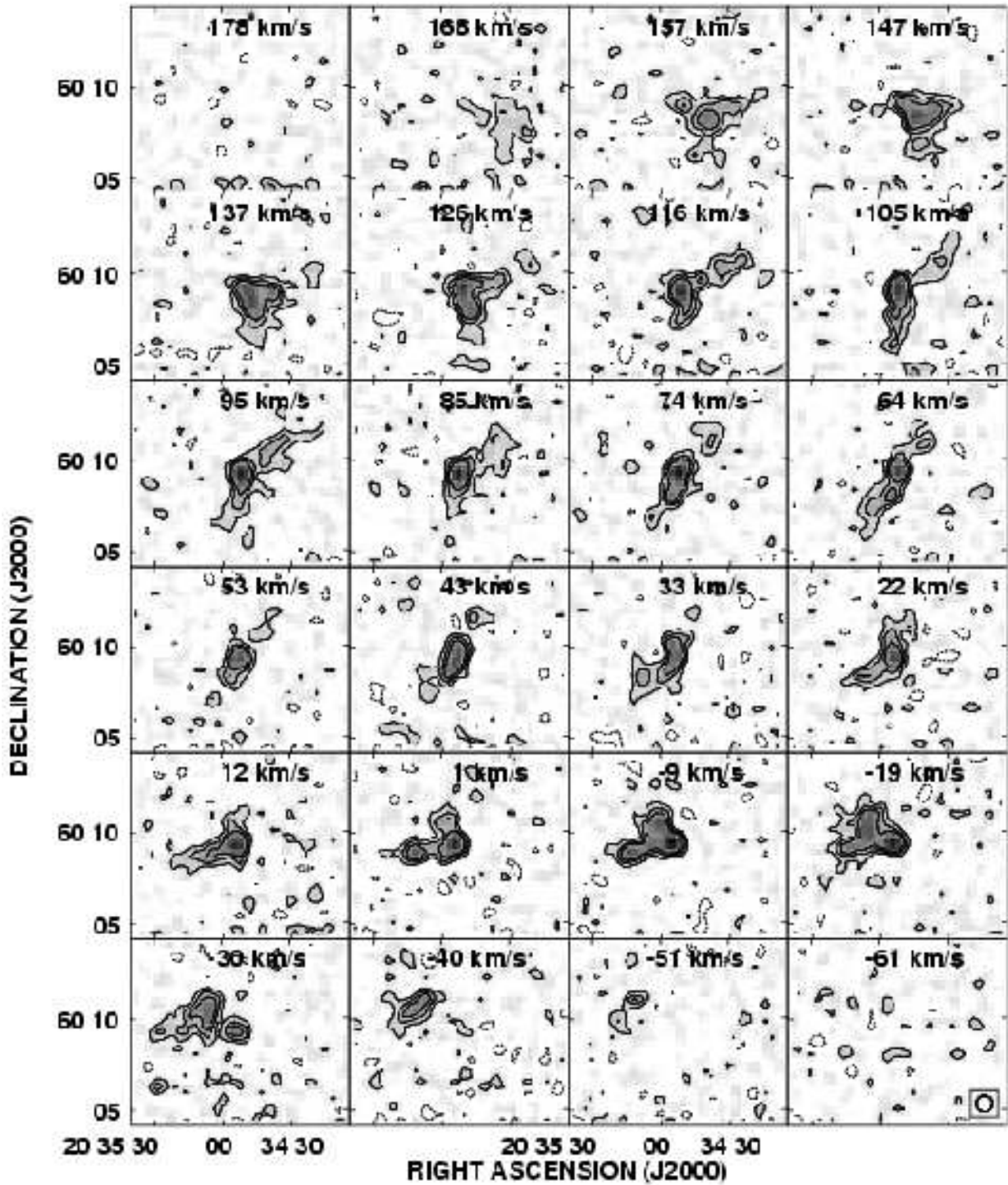


Fig. 1.— CO(1-0) channel maps for NGC 6946. Grey scale ranges from 0 to 0.54 K. Contours are at -0.070, 0.070, 0.14 and 0.21 K. The rms noise in a channel with no emission is 0.033 K. The 55'' (FWHM) circular beam is displayed in the -61 km s^{-1} channel at the lower right. Each channel is labeled with the channel velocity (LSR). The channels are separated by 10.4 km s^{-1} .

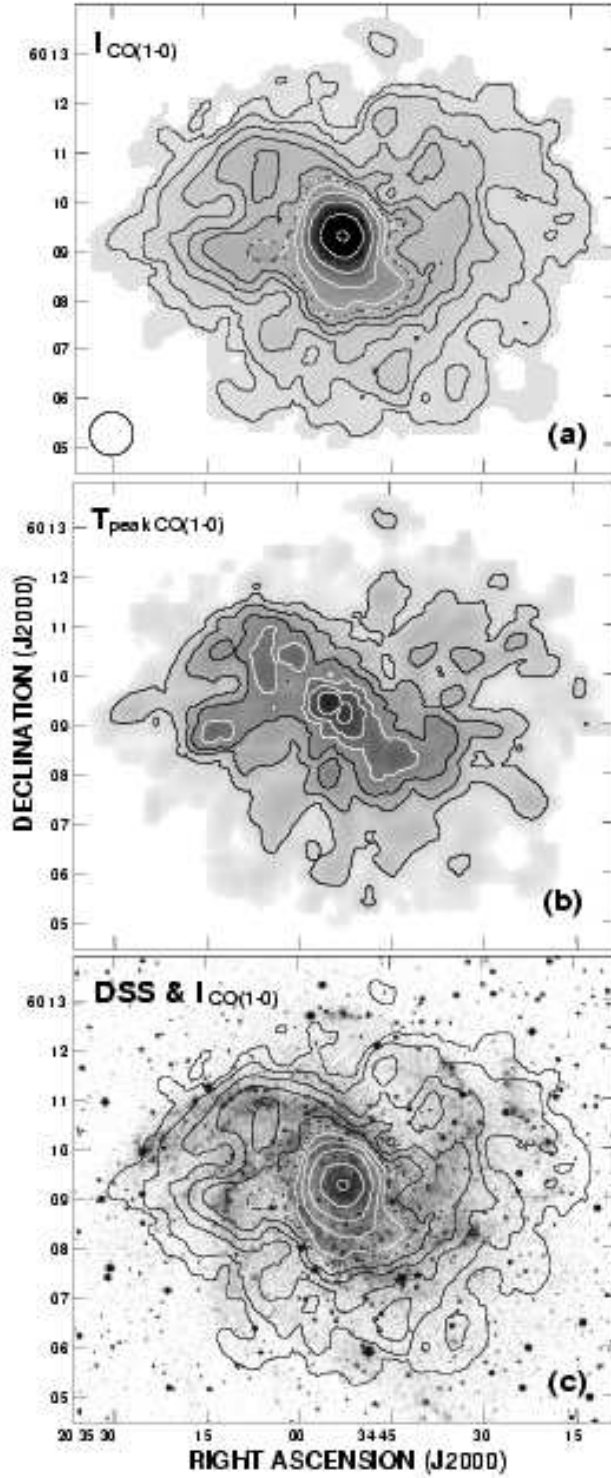


Fig. 2.— CO(1-0) integrated and peak intensity maps for NGC 6946. a) CO(1-0) integrated intensity map. Grey scale ranges from 0 to 50 K km s^{-1} . The contour levels are 1, 2.5, 5, 7.5, 10, 12.5, 15, 20, 30, 50, and 70 K km s^{-1} . The 55" (FWHM) circular beam is displayed at the lower left. b) CO(1-0) peak intensity map. Grey scale ranges from 0 to 0.52 K. The contour levels are 0.10, 0.17, 0.23, 0.30, 0.37 and 0.43 K. c) DSS uncalibrated optical image with the same I_{10} contours shown in (a).

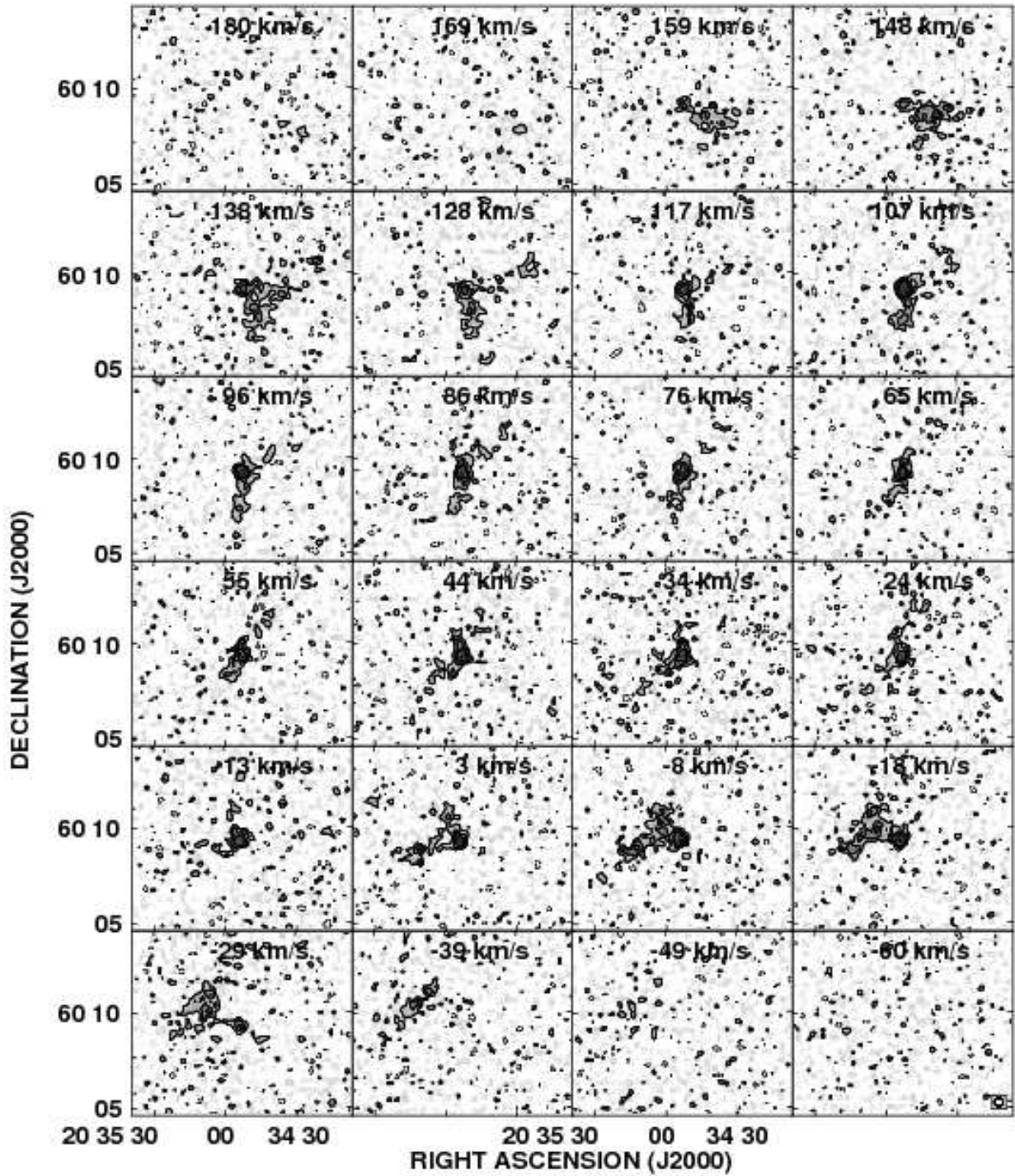


Fig. 3.— CO(2-1) channel maps for NGC 6946. Grey scale ranges from 0 to 0.85 K. Contours are at -0.17 , 0.17 , 0.34 and 0.51 K. The rms noise in a channel with no emission is 0.085 K. The $27''$ (FWHM) circular beam is displayed in the -60 km s $^{-1}$ channel at the lower right. Each channel is labeled with the channel velocity (LSR). The channels are separated by 10.4 km s $^{-1}$.

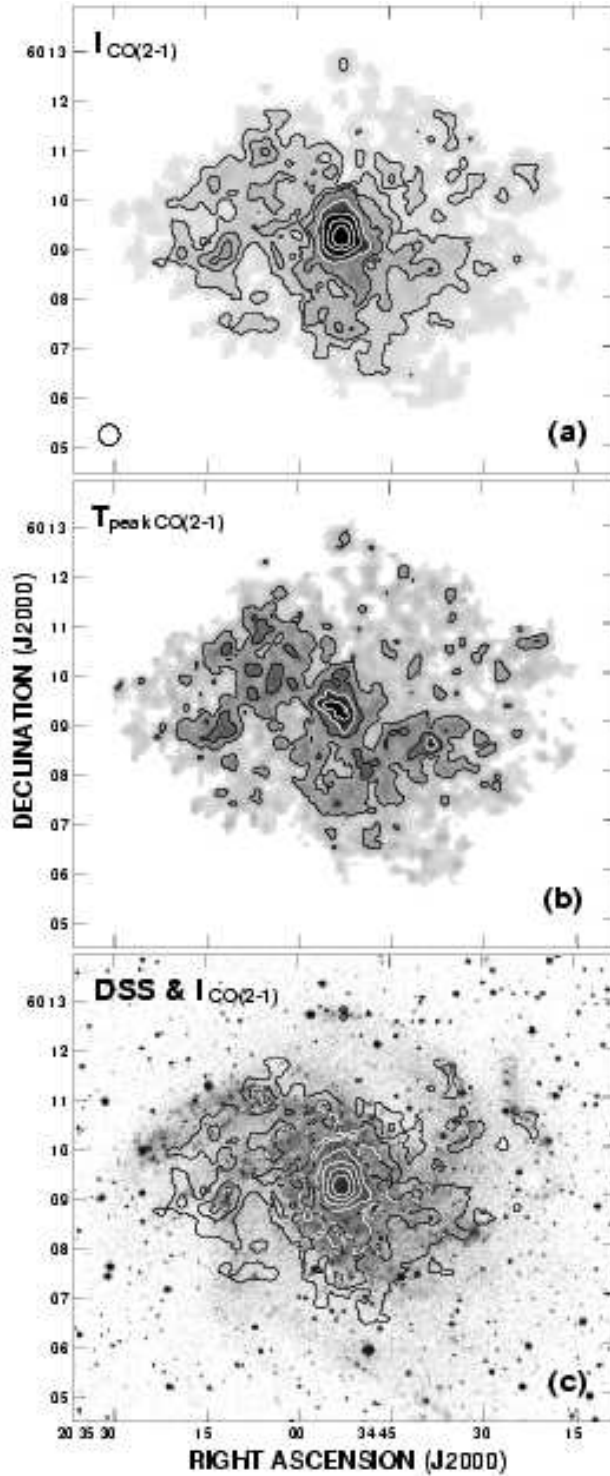


Fig. 4.— CO(2-1) integrated and peak intensity maps for NGC 6946. a) CO(2-1) integrated intensity map. Grey scale ranges from 0 to 50 K km s^{-1} . The contour levels are 5, 10, 15, 30, 50, 75, and 100 K km s^{-1} . The $27''$ (FWHM) circular beam is displayed at the lower left. b) CO(2-1) peak intensity map. Grey scale ranges from 0 to 0.8 K. The contour levels are 0.26, 0.43, 0.60 and 0.77 K. c) DSS uncalibrated optical image with the same I_{21} contours shown in (a).

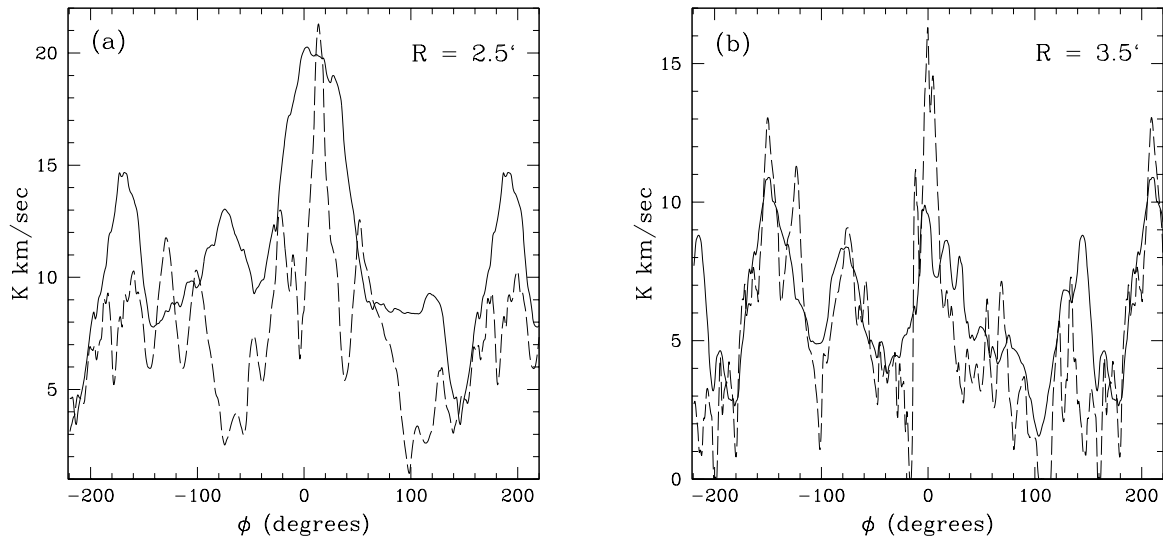


Fig. 5.— Azimuthal plots of CO in NGC 6946 at selected radii. The I_{CO} maps were transformed to face-on images and the azimuthal variation in I_{CO} was measured at constant galactic radii. Due south is at $\phi = 0^\circ$, west is at $\phi = 90^\circ$. CO(2-1) is traced by the dashed line, CO(1-0) by the solid line. The data are presented at their native beam sizes, $27''$ and $55''$, for the CO(2-1) and CO(1-0) respectively. a) The azimuthal variation at $R = 2.5'$ (4.4 kpc). b) The azimuthal variation at $R = 3.5'$ (6.1 kpc).

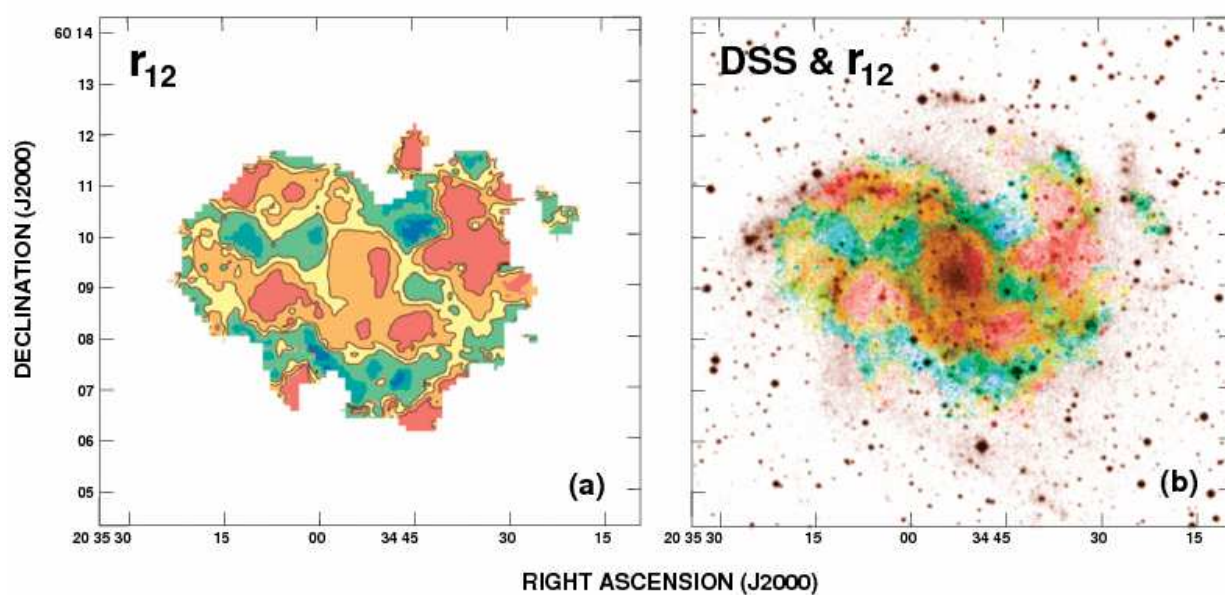


Fig. 6.— The CO(2-1)/CO(1-0) ratio in NGC 6946. a) $r_{12} = I_{21}/I_{10}$. The contours are at $r_{12} = 0.8, 1.0$ and 1.2 . For the colored regions: red represents $r_{12} < 0.8$; orange for $0.8 > r_{12} > 1.0$; yellow for $1.0 > r_{12} > 1.2$; green for $r_{12} > 1.2$; blue for $r_{12} \sim 2$. b) Digital Sky Survey optical image with r_{12} in color. The color scheme roughly follows that of figure a) and is intended to show the relationship between the regions of high/low r_{12} and the optical stellar disk.

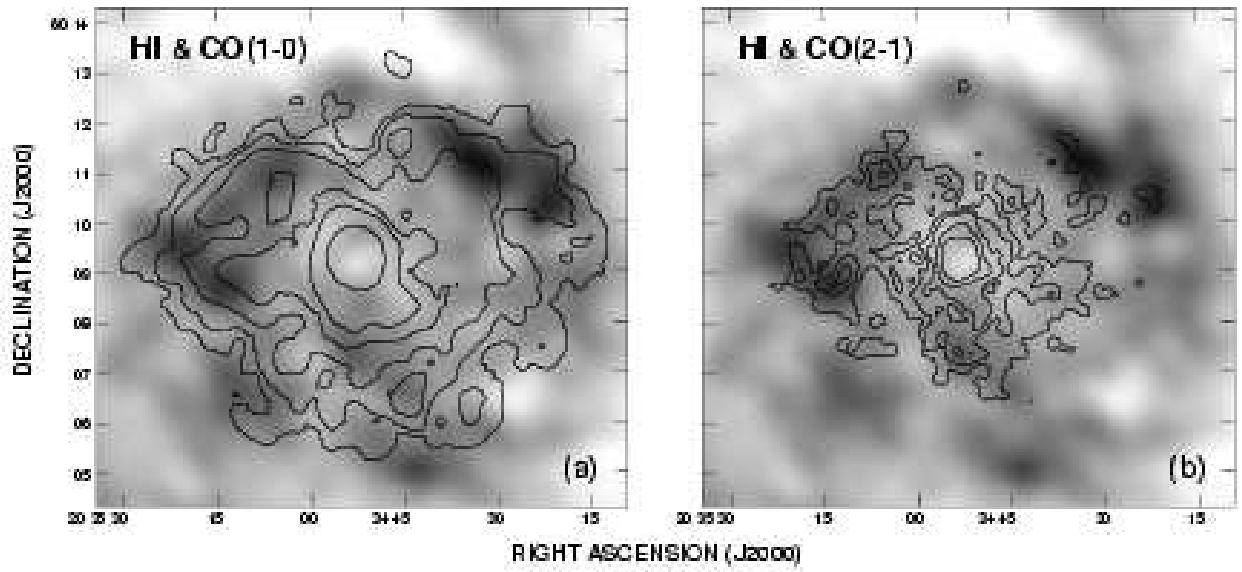


Fig. 7.— CO and HI in NGC 6946. a) I_{HI} (grey) and I_{10} (contours). Grey scale ranges from 0.5 to $3.7 \text{ Jy beam}^{-1} \text{ km s}^{-1}$. The I_{10} contours and are at 1, 2.5, 5, 10, 15 and 35 K km s^{-1} . b) I_{HI} (grey) and I_{21} (contours). Grey scale ranges from 0 to $3.7 \text{ Jy beam}^{-1} \text{ km s}^{-1}$. The I_{21} contours and are at 5, 10, 15, 30 and 50 K km s^{-1} .

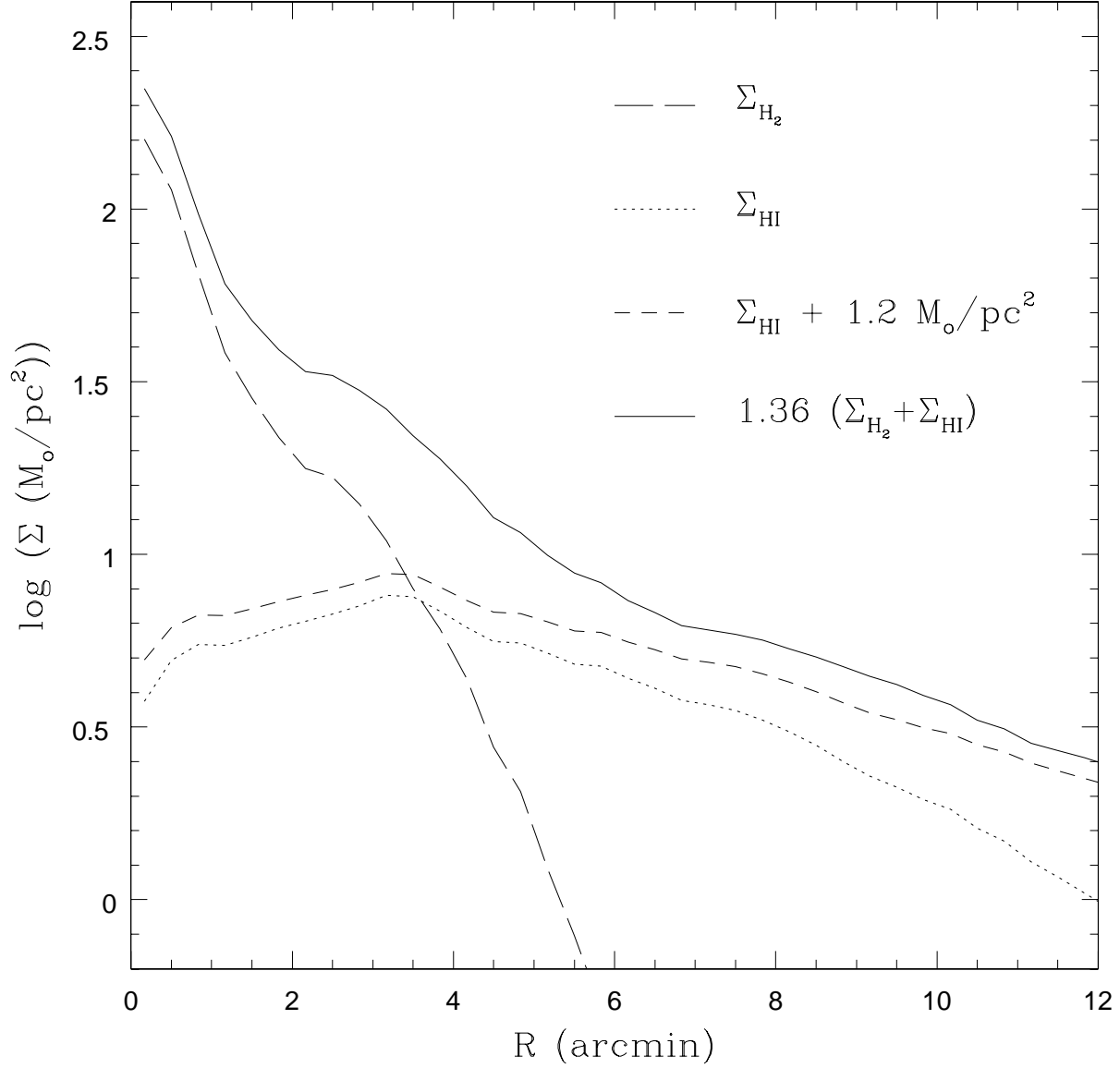


Fig. 8.— Gas surface density vs radius in NGC 6946. Plotted are: Σ_{H_2} derived using the standard conversion factor; Σ_{HI} from the observed emission; Σ_{HI} increased for the VLA missing flux estimate; and the total gas surface density increased by a factor of 1.36 to include the He and heavier element content. All have been corrected for inclination, $(\cos i)$. At our assumed distance of 6 Mpc, $1' = 1.75$ kpc.

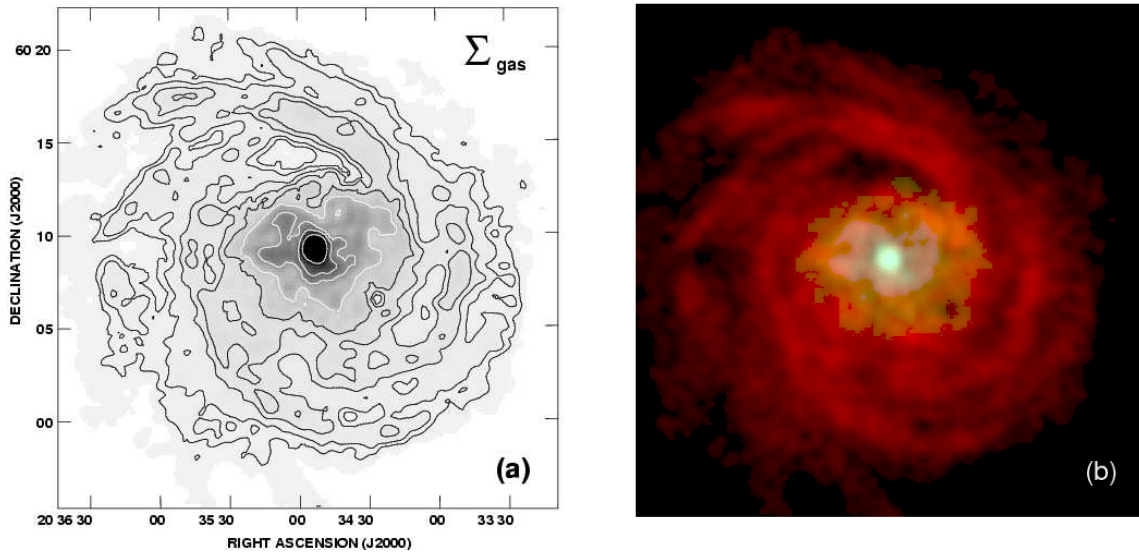


Fig. 9.— The neutral gas surface density in NGC 6946. a) A map of the total neutral gas surface density, corrected for inclination ($\cos(40^\circ)$) and increased by a factor of 1.36 for the He and heavier element content. This map does not include a missing HI flux estimate. Contours are at 1, 2, 4, 6, 10, 20, 40, 60 and 100 $M_{\odot} \text{pc}^{-2}$. b) A false color image with CO(1-0) in green and HI in red. Regions of nearly equivalent column densities show up in orange. The CO(2-1) emission has been added in blue to bring out the bright CO nucleus.

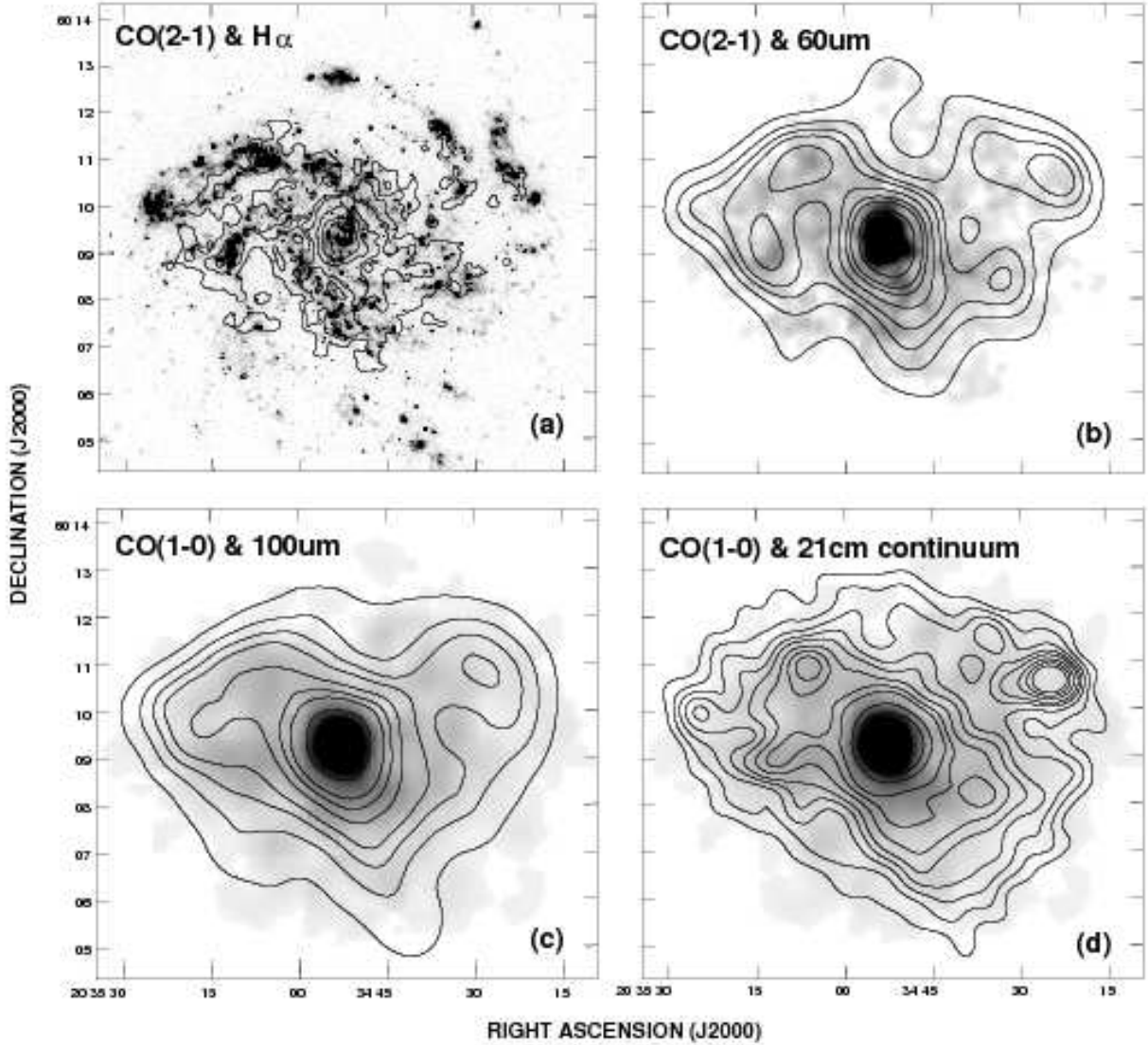


Fig. 10.— CO and star formation tracers in NGC 6946. The CO(1-0) and CO(2-1) beam sizes are $55''$ and $27''$ respectively. a) I_{21} in contours and $H\alpha$ in grey. The $H\alpha$ image is from Ferguson et al. (1998) and is not presented here in calibrated units. The $H\alpha$ image was regridded to $2''$ pixels. The I_{21} contours are at 5, 10, 15, 30, and 50 K km s^{-1} . b) I_{21} in grey with IRAS 60 μm contours. The grey scale ranges from 0 to 40 K km s^{-1} . The 60 μm contours are at 10, 20, 30, 40, 60, 90, 120 and 200 MJy sr^{-1} . The 60 μm beam size (FWHM) is $45'' \times 41''$, $pa = 21^\circ$ and the rms noise level is 0.6 MJy sr^{-1} . c) I_{10} in grey with IRAS 100 μm contours. The grey scale ranges from 0 to 40 K km s^{-1} . The 100 μm contours are at 20, 40, 60, 80, 120, 160, 200 and 300 MJy sr^{-1} . The 100 μm beam size (FWHM) is $69'' \times 65''$, $pa = 20^\circ$ and the rms noise level is 2 MJy sr^{-1} . d) I_{10} in grey with 21 cm continuum contours. The grey scale ranges from 0 to 40 K km s^{-1} . The 21 cm contours are at 5, 7, 10, 12, 18, 22, 25, 36 and 48 mJy beam^{-1} . The beam size size (FWHM) is $49'' \times 42''$, $pa = 73^\circ$ and the rms noise level is 1.2 mJy beam^{-1} .

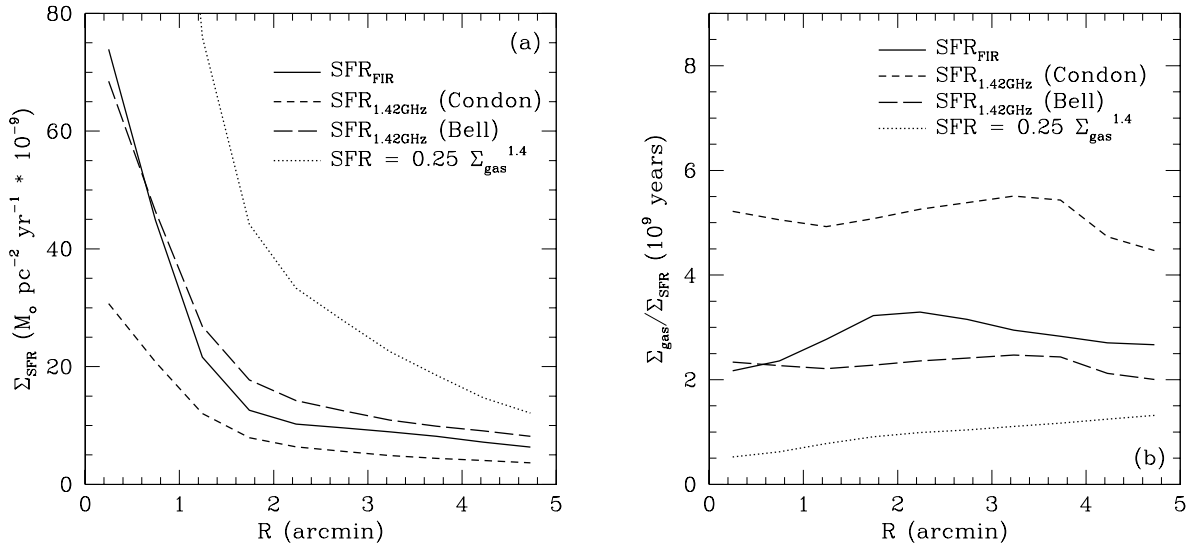


Fig. 11.— Radial star formation rates and efficiencies in NGC 6946. a) Σ_{SFR} derived from the IRAS luminosities, L_{fir} ; non-thermal radio continuum luminosity, L_{ntc} , using the SFR calibration of Condon (1992), and L_{ntc} using the SFR calibration from Bell (2003); and as predicted by Schmidt law of Kennicutt (1998a) from Σ_{gas} . b) The star formation efficiency expressed in terms of τ_{SFE} , the time it would take to consume all of the molecular gas at the given star formation rate. The legends in both figures indicate the source of the SFR calibration. At our assumed distance of 6 Mpc, $1' = 1.75$ kpc.

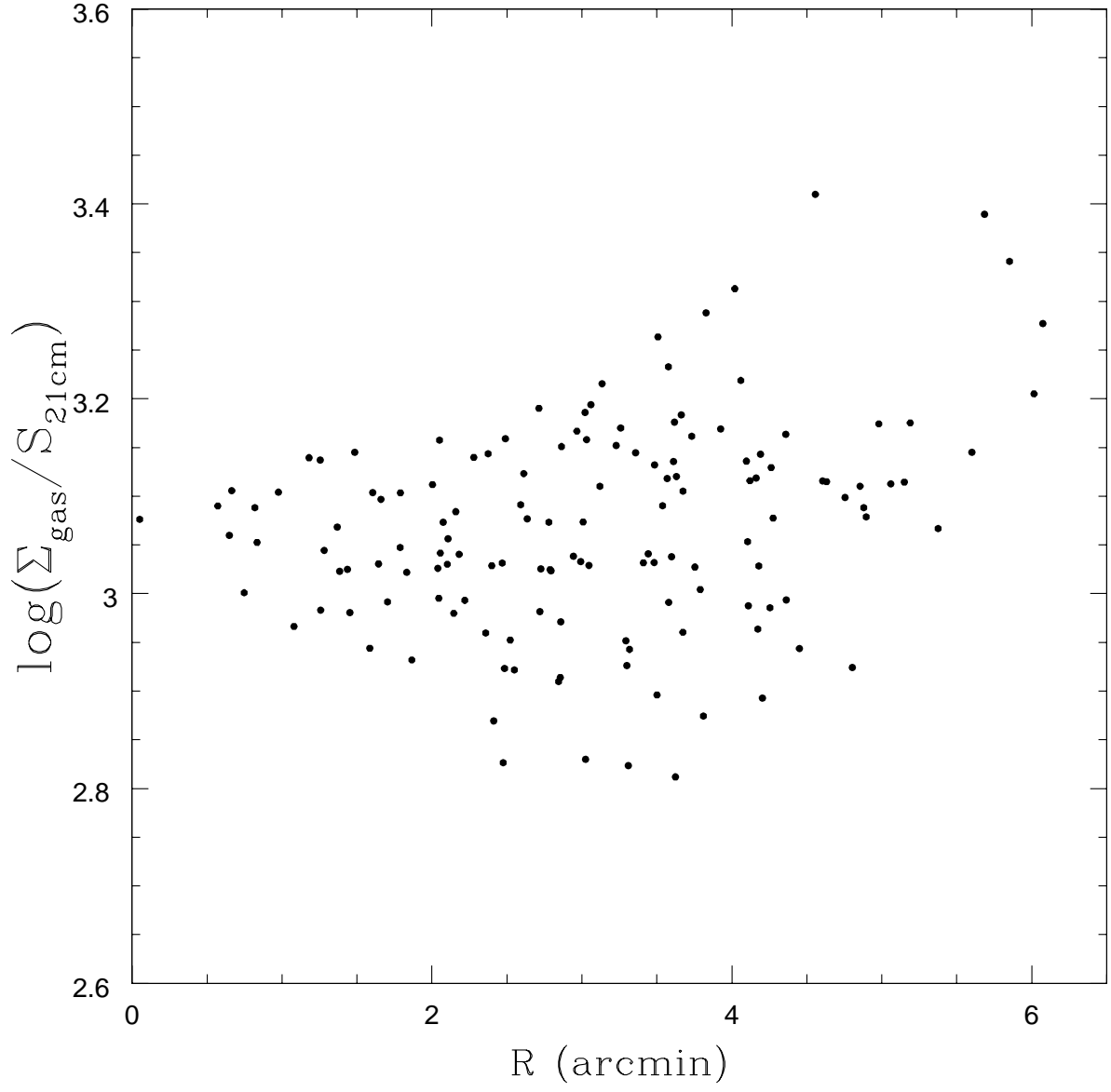


Fig. 12.— Ratio of total gas surface density to 21 cm continuum in NGC 6946. The gas surface density maps was convolved to a $70''$ FWHM beam size and clipped at a 3σ level prior to forming the ratios. The resulting ratio maps were sampled on a $35''$ grid. At our assumed distance of 6 Mpc, $1' = 1.75$ kpc.

Table 1. Global Properties of NGC 6946

Property	Value
Hubble type ^a	Scd
R.A. (J2000) ^b	20 ^h 34 ^m 51. ^s 6 ($\pm 0.s4$)
Dec. (J2000) ^b	60° 9' 8.7'' ($\pm 1.6''$)
l^{II}, b^{II} ^a	95.7°, 11.7°
Distance ^c	6 Mpc
v_{LSR} ^d	50.5 (± 1.3) km s ⁻¹
Inclination ^d	40° ($\pm 10^\circ$)
Position Angle ^d	242° ($\pm 1^\circ$)
V_{max} ^d	170 (± 40) km s ⁻¹
$R_{V_{max}}$ ^d	5.1' ($\pm 0.7'$) (9.0 kpc)
n ^d	1.07 (± 0.07)
$M_{H2\ total}$ ^e	$3.3 \times 10^9 M_\odot$
$M_{HI\ observed}$ ^f	$5 \times 10^9 M_\odot$
M_{HI} ^g	$7 \times 10^9 M_\odot$
M_{gas} ^h	$1.4 \times 10^{10} M_\odot$
M_{dyn} ⁱ	$1.9 \times 10^{11} M_\odot$

^aobtained from the NASA/IPAC Extragalactic Database.

^bdynamical center based on fit of Brandt rotation model to the HI data.

^cSharina et al. (1997).

^dkinematic parameters from fit of Brandt rotation model to the HI data.

^edetected, using a 2.0×10^{20} K km s⁻¹ conversion factor.

^fdetected, no VLA missing flux estimate.

^gincludes VLA missing flux estimate.

^hincludes factor for He and heavier elements: $1.36(M_{H2} + M_{HI})$.

ⁱtotal dynamical mass based on Brandt model fit parameters.

Table 2. Properties of 3 Late-type Galaxies and the Milky Way

Galaxy	IC342 ^a	NGC 6946	M83 ^b	Milky Way
Hubble type	Scd	Scd	SBc	SBbc
Distance (Mpc)	3.3 ^c	6	4	...
D_{H_2} (arcminutes) ^d	20	11	11	...
D_{H_2}/D_{HI}	0.23	0.38	0.15	...
D_{H_2}/D_{25} ^e	1.1	1.0	1.0	...
$M_{dynamical}$ ($10^{11} M_{\odot}$)	1.8 ^f	1.9	0.7	~ 3 ^g
$M_{H_2 total}$ ($10^8 M_{\odot}$)	16 ^{h,i}	33	23 ⁱ	25 ^j
$M_{HI total}$ ($10^8 M_{\odot}$) ^k	57 ^h	70	62	48 ^l
M_{H_2}/M_{HI}	0.27	0.47	0.37	0.52
M_{gas}/M_{dyn} ^m	0.055	0.074	0.16	0.03
$\Sigma_{H_2}^{nucleus}$ ($M_{\odot} \text{ pc}^{-2}$) ⁿ	140	170	220	400 ^o
$\Sigma_{H_2}^{disk}$ ($M_{\odot} \text{ pc}^{-2}$) ^p	11	13	23	3.4 ^q

^adata from Crosthwaite et al. (2000,2001).

^bdata from Crosthwaite et al. (2002).

^clatest distance estimate based on Cepheid variables Saha et al. (2002).

^dusing the radius at which the azimuthal average $\Sigma_{H_2} \sim 0.5 M_{\odot} \text{ pc}^{-2}$.

^e D_{25} from RC2, de Vaucouleurs, de Vaucouleurs & Corwin (1976).

^fdynamical mass from Brandt model using 3.3 Mpc adjusted from 2 Mpc.

^gwithin 20 kpc, Nikiforov et al. (2000), from rotation curve modeling.

^hadjusted to 3.3 Mpc distance from 2 Mpc.

ⁱrescaled to a $2.0 \times 10^{20} \text{ K km s}^{-1}$ conversion factor.

^jCombes (1991).

^kincludes VLA missing flux estimates.

^lKulkarni & Heiles (1987).

^mgas includes factor of 1.36 for He and heavier elements.

ⁿ $M_{\odot} \text{ pc}^{-2}$ in $55'$ beam centered on the nucleus.

^o $R < 400 \text{ pc}$, Scoville & Sanders (1987).

^pmean Σ_{H_2} from observed CO disk excluding the nucleus.

^q400 pc < R < 14 kpc, Scoville & Sanders (1987).

Table 3. Radial Slope of Gas to Star Formation Tracer Ratios

Gas Tracer ^a	SF Tracer ^a	Slope (Uncertainty) ^b
I_{21}	100 μm	-0.196 (0.015)
I_{21}	60 μm	-0.189 (0.015)
I_{21}	21 cm continuum	-0.170 (0.014)
I_{21}	H α	-0.224 (0.015)
I_{10}	100 μm	-0.102 (0.008)
I_{10}	60 μm	-0.095 (0.009)
I_{10}	21 cm continuum	-0.076 (0.009)
I_{10}	H α	-0.130 (0.014)
Σ_{gas}^c	100 μm	-0.002 (0.006)
Σ_{gas}	60 μm	0.005 (0.007)
Σ_{gas}	21 cm continuum	0.024 (0.007)
Σ_{gas}	H α	-0.030 (0.013)

^aMaps were convolved to a 70'' circular beam size and clipped at 3σ . The region containing the bright 21 cm continuum emission, tentatively identified as a background galaxy, at $\alpha = 20^h 34^m 24.9^s$ $\delta = 60^\circ 10' 38''$ (J2000) was clipped from all the comparison maps.

^bSlope (ratio/arcminute) and rms uncertainty from a least squares fit to the ratio of gas tracer to formation tracer as a function of galactic radius, $\log(\text{Gas}_{tracer}/\text{SF}_{tracer}) = A \cdot r + B$. The maps were sampled on a grid of half beam width points (35'').

^cThe molecular gas surface density derived from CO plus the atomic gas surface density derived from HI, increased by a factor of 1.36 to account for He and heavier elements.

Table 4. Comparison of the Milky Way and NGC 6946 at Large R

	Milky ^{a,b}			NGC ^c		
	Way	8 kpc	12 kpc	6946	8 kpc	12 kpc
N_{HII}/kpc^2		21	> 1.4		~ 5 ^d	~ 1 ^d
$\Sigma_{H_2}(\text{M}_\odot \text{pc}^{-2})$		2.9	> 0.15		2.3 ± 1.7	.. ^e
$\Sigma_{HI}(\text{M}_\odot \text{pc}^{-2})$		2.9	2.9		7-9 ^f	3-5 ^f

^ausing $R_\odot = 8$ kpc.

^bvalues from discussion in Wouterloot et al. (1988)

^cusing distance to NGC 6946 = 6 Mpc.

^dthe HII region positions from Hodge & Kennicutt (1983) were sampled on a grid of points separated by $10''$. The points were regrouped into $20''$ wide galactic radius bins. The 12 kpc value was extrapolated from the resulting N_{HII}/kpc^2 curve.

^ebeyond our measured CO disk.

^fincluding the estimated flux missing from the VLA map would increase these by $1.2 \text{ M}_\odot \text{pc}^{-2}$.